Frequency-Constrained Autonomous Microgrid Planning for Mining Industry Applications

Hossein Ranjbar*, Hirad Assimi, S. Ali Pourmousavi, Wen L. Soong

School of Electrical and Mechanical Engineering, University of Adelaide, Adelaide, Australia

Abstract

This paper presents a new frequency-constrained microgrid (MG) planning methodology for mining industry with a high penetration of renewable energy sources (RES). The proposed model is formulated as a multi-objective bi-level optimisation problem in which the upper-level (UL) problem aims to minimise the total net present cost (NPC) of the MG, mitigate the greenhouse gas (GHG) emissions, and improve system reliability. In the lower-level (LL) problem, the operation of the MG is simulated considering unit commitment, battery operation, and frequency stability constraints. The non-dominated sorting genetic algorithm II (NSGA-II) is employed to solve the UL multi-objective optimisation problem, generating candidate solutions that define the MG's energy source capacities. Each candidate solution is evaluated by solving the LL problem, formulated as a mixed-integer linear programming (MILP) problem and solved using Gurobi solver. This iterative process ensures accurate evaluation of operational costs and emissions while exploring trade-offs between objectives. The fuzzy decision-making method is then applied to the Pareto optimal solutions to obtain the final optimal plan. Through this model, optimal capacities of RES units, battery energy storage systems (BESSs), and back-up fossil fuel generators are obtained to meet the MG demand. Moreover, the proposed approach ensures that the frequency stability requirements, including rate of change of frequency (RoCoF), minimum/maximum frequency and steady-state frequency remain within acceptable thresholds after considering any imbalance events. Finally, the simulation study is conducted to validate the effectiveness of the proposed model using a real-world MG in a remote underground mine in Australia utilising historical load, expected RES generation, and commodity/capital price data. The results demonstrate that the proposed model effectively ensures compliance with frequency stability requirements—always maintaining frequency above 49.5 Hz and RoCoF below 0.5 Hz/s—while achieving a balanced trade-off between cost and emissions. Compared to the conventional approach, the proposed solution results in a slightly higher NPC (2.8%) and GHG emissions (4.5%), but significantly reduces RES curtailment (13%) and eliminates severe frequency deviations, which in the conventional case occurred 60% of the time with drops as low as 48.9 Hz and RoCoF

as high as 0.875 Hz/s. This highlights the critical role of BESS in enhancing both economic performance and frequency stability in off-grid mining MGs.
Keywords: Renewable energy sources, frequency stability, mining industry, microgrid, energy storage system.

Nomenclature

A. Sets and indices

Ψ	Set of microgrid energy sources, indexed by i
E	Set of representative days, indexed by e
G	Set of diesel generators, indexed by g
K_i	Set of components of energy source i with salvage value, indexed by k
T	Set of time intervals in a day, indexed by t
y	Index of year

B. Parameters

$\Delta PL_{t,e}^{max}$	Power imbalance at time t on representative day e before battery action [MW]
$\Delta T'$	Time interval length of primary frequency response [h]
ΔT	Time interval length of normal operation [h]
η^{ch}, η^{dis}	Charging and discharging efficiency of the battery
$\Gamma, \Lambda, \Upsilon$	Penalty factors for RES curtailment and load shedding before and during frequency response [$/MWh]
$\overline{ENS}$	Maximum energy not served allowed [MWh/yr]
$\overline{P_{t,e}^{pv}}, \overline{P_{t,e}^{wt}}$	Predicted normalised solar and wind power generation at time t on representative day e [0-1]

*Corresponding author.Tel: +61458890131
Email addresses: hossein.ranjbar@adelaide.edu.au (Hossein Ranjbar), hirad.assimi@adelaide.edu.au (Hirad Assimi), a.pourm@adelaide.edu.au (S. Ali Pourmousavi), wen.soong@adelaide.edu.au (Wen L. Soong)

π_e	Number of days in the representative day e cluster in a year
a_g, b_g	Generation cost parameters of generator g [\$/MWh, \$/h]
c_g^I	Capital cost of diesel generator g [\$/MW]
c_g^r	Cost of primary reserve of generator g [\$/MWh]
c_i^I	Capital cost of renewable unit i [\$/MW]
c_i^O	Operation and maintenance cost factor of renewable unit or BESS i [\$/MW-yr]
$c_{\mathtt{ec}}^I$	Capital cost and lifetime of BESS energy unit [\$/MWh, yr]
$c_{\mathtt{in}}^I, L_{\mathtt{in}}$	Capital cost and lifetime of solar inverter [\$/MW, yr]
$c_{\mathtt{md}}^I$	Capital cost of PV module [\$/MW]
$c_{\mathtt{nc}}^I, L_{\mathtt{nc}}$	Capital cost and lifetime of wind turbine nacelle [\$/MW, yr]
$c_{\mathtt{pc}}^I, L_{\mathtt{pc}}$	Capital cost and lifetime of power conversion system of BESS [\$/MW, yr]
$c_{\mathtt{rt}}^I, L_{\mathtt{rt}}$	Capital cost and lifetime of wind turbine rotor [\$/MW, yr]
c_{BT}^d	Cost of BESS degradation based on energy throughput [\$/MWh]
c_{BT}^p, c_{BT}^e	Capital cost of power and energy components of BESS [\$/MW, \$/MWh]
c_g^M, c_g^F	Maintenance and fuel cost factors of diesel generator g [\$/MW-yr, \$/MWh]
$c_{rate}^{min}, c_{rate}^{max}$	Minimum and maximum c-rating of BESS [MW/MWh]
em_g	Per unit emission of diesel generator g [kg CO_2-e/MWh]
EoL	End-of-life fraction of battery
f^0	Nominal frequency [Hz]
f^{db}	Governor deadband of generator g [Hz]
f^{min}, f^{max}	Minimum and maximum acceptable frequency [Hz]
$f_{PV}, W_{\mathtt{md}}$	Failure rate of PV modules and their warranty period in years
H_g	Inertia constant of generator g [MW.s/MW]

ir	Compound interest rate
$L_{k,i}$	Lifetime of component k of DER i [yr]
L_{mg}	MG lifetime [yr]
P_g^{min}, P_g^{max}	Minimum and maximum power generation of generator g [MW]
P_i^{max}	Maximum installed power capacity of DER i [MW]
$Pd_{t,e}$	Amount of load demand at time t on representative day e [MW]
R_g^{max}	Maximum primary reserve from generator g [MW]
$RoCoF^{max}$	Maximum acceptable RoCoF value [Hz/s]
RU_g, RD_g	Maximum ramp up and ramp down rates of generator g [MW/h]
$SoE^{min/max}$	Minimum/maximum limits of state of energy of the BESS [0-1]
UT_g, DT_g	Minimum up and down times of generator g [h]
v_g	Maximum ramp rate of the governor of generator g [MW/s]

C. Variables

$\Delta E_{t,e}$	Amount of energy that battery must be able to provide at time t on representative day e to help deal with the post-contingency frequency deviation [MWh]
$\Delta f(t)$	Frequency deviation [Hz]
$\Delta P_{t,e}^{ns}$	Amount of load not served during primary frequency response (PFR) at time t on representative day e [MW]
$\Delta PB_{t,e}$	Available capacity of battery at time t on representative day e post contingency [MW]
$\Delta PL_{t,e}$	Amount of power imbalance at time t on representative day e after battery action [MW]
$E_{g,yr}$	Total energy production of diesel generator g per year [MWh]
$H_{t,e}$	System inertia after contingency at time t on representative day e [MW.s/Hz]
P_g^{max}	Installed power capacity of diesel generator g [MW]

P_i	Installed power capacity of renewable unit i [MW]
P_{BT}, E_{BT}	Installed power and energy capacity of BESS [MW, MWh]
$P_{g,t,e}$	Power output of diesel generator g at time t on representative day e [MW]
$P_{t,e}^{bt,max}$	Maximum available charge and discharge power of battery at time t on representative day e post contingency [MW]
$P_{t,e}^{dis}, P_{t,e}^{ch}$	Discharging and charging power of the battery at time t on representative day e [MW]
$P_{t,e}^{ns}$	Amount of load not served at time t on representative day e [MW]
$P_{t,e}^{RES,cu}$	Total power curtailment of renewable units at time t on day e [MW]
$P_{t,e}^{WT}, P_{t,e}^{PV}$	Power production of wind and solar PV units at time t on representative day e [MW]
$R_{g,t,e}$	Available primary reserve from generator g at time t on representative day e [MW]
$SoE_{0,e}$	Initial state of energy of the BESS on representative day e [MWh]
$SoE_{t,e}$	State of energy of the BESS at time t on representative day e [MWh]
$T_{g,t,e}^{ON}, T_{g,t,e}^{OFF}$	Number of consecutive ON and OFF times of generator g at time t on representative day e [h]
$u_{g,t,e}$	Binary variable associated with on/off status of generator g at time t on representative day e [0,1]
$Z_{t,e}$	Binary variables to apply complementarity condition on BESS operation at time t on representative day e [0,1]

1. Introduction

1.1. Background and Motivation

Mining industry is an energy-intensive sector highly dependent on fossil fuels, both in its early development stages and throughout its operational life. Energy consumption within the mining industry accounts for approximately 38% of all industrial energy use globally and approximately 11% of global energy consumption [1]. This substantial energy consumption is projected to double by 2050 without the implementation of

new policy measures [2]. In Australia, the mining industry is responsible for approximately 14% of the total energy consumption of the country, with a significant portion of this energy derived from fossil fuels [1, 3]. As [4] indicates, the mining industry accounts for approximately 4% to 7% worldwide and approximately 11% of total Australia's greenhouse gas (GHG) emissions, largely due to its high energy consumption. This results in significant energy costs in the mining sector, which can account for as much as 30% of operating costs [5].

Consequently, the mining industry is actively moving towards decarbonisation and electrification through the integration of renewable energy sources (RES) and battery electric vehicles (BEVs) to reduce fossil fuel consumption and GHG emissions, driven by environmental regulations and social pressures [1, 6, 7]. However, serious questions about the energy source for charging BEVs have been raised, given Australia's mining industry's heavy dependence on fossil fuels, where approximately 74% of its energy comes from diesel and gas [3, 7, 8]. This issue will be more critical given that approximately 35% of the total operating mines in Australia are off-grid, with 65% of these located in Western Australia [9]. For example, charging battery-powered mining equipment, such as haul trucks, can significantly affect mining microgrid (MG) design and operation due to the high peak loads (e.g., MW range) and high ramp rates [10, 11]. This presents a significant challenge for mining MG in particular, as the majority function standalone without connection to the main grid. For example, the Epiroc MT42 battery-powered truck contains 375 kWh of batteries [12]. The truck can be charged through a fast charger at a 2C rate equivalent to 750 kW, placing considerable power demand on the mining MG. Because the truck is equipped with two electric motors with a total nominal power of 400 kW, it can fully discharge the battery in approximately 1 hour at rated power before recharging is needed. As a result, battery charging can present a significant demand on the MG, which regularly cycles on and off during a 12-hour shift. These load fluctuations cause significant disturbances in the network, manifesting as fluctuations in frequency and voltage, especially in remote mining locations.

Furthermore, incorporating large-scale RES in mining MG introduces complexities in managing variable load profiles and ensuring compatibility with the intermittent nature of RES generation [1, 6]. For instance, it could threaten the stability of the MG when faults or disturbances occur due to the reduction in the inertia of the MG [13]. Hence, large frequency deviations can occur more frequently considering the lower inertia of the system and increasingly uncertain RES generation, especially in mines with many fast chargers due to electrification. To this end, an optimised MG consisting of a high share of RES, battery energy storage systems (BESSs), and fossil fuel backup generators is crucial to provide an uninterrupted power supply and meet the energy demand in mines considering frequency stability constraints.

1.2. Literature Review

Numerous studies on MG design frameworks and methodologies are available for typical use cases of residential, commercial, and community MGs, both in grid-connected and off-grid modes, to minimise total costs and emissions. For instance, [14] and [15] presented frameworks for designing off-grid residential MGs consisting of solar, wind, BESSs, and diesel generators to meet the demand in the rural areas of Algeria and Morocco at the lowest cost. In [16] and [17], multi-objective optimisation models were proposed for sizing grid-connected MG components to minimise both total costs and emissions.

However, there is a limited body of literature on MG applications in the mining industry, which is a unique industry in terms of its high energy intensity, remote and off-grid operational locations, reliance on heavy machinery with specific power requirements, the need for robust solutions to support reliable continuous 24/7 operations, and scalability to meet fluctuating energy demands as mine production level changes over time. In [18], a framework for optimal off-grid MG sizing was proposed to analyse the profitability of RES, which was tested in three Australian mines. The authors in [19] performed a techno-economic analysis to evaluate the feasibility of integrating concentrated solar power (with thermal storage) and solar PV systems (combined with battery storage) to provide energy for a typical mine in Zimbabwe. A multi-objective model was presented in [20] for optimal sizing of grid-connected MG consisting of solar-biogas RES and energy storage systems to minimise total costs and GHG emissions at the mine sites. The work in [2] evaluated the economic potential of hybrid MGs in mining using the HELiOS mining model, considering technical, economic, and spatial factors. It focused on grid-connected and off-grid mines in Northern Chile and off-grid mines in Northwestern Australia and Yukon, Canada.

Furthermore, increasing penetration of RES, particularly wind and solar, is displacing conventional synchronous units that provide the essential inertia and primary frequency response (PFR), thus reducing the total inertia of the system and making frequency management more challenging [21, 22]. In this regard, some studies developed energy management and operation frameworks for MGs considering the frequency stability requirements. For instance, the authors in [23] developed a frequency-constrained energy management system to handle the frequency deviation arising from the short-term power fluctuations of RES in off-grid MGs. In [24], a two-stage stochastic model was proposed to formulate the frequency-constrained unit commitment problem considering the reserve provision from wind turbines. The authors in [25] developed a proactive scheduling model for grid-connected MGs considering the frequency dynamics after islanding. In [26], a frequency-constrained scheduling model was proposed for integrated electricity-heat MGs considering the distributionally robust joint chance constraint method for handling the uncertainties.

However, there is a few studies that have focused on the sizing of MGs considering PFR and inertia support constraints. In [27], a mixed-integer linear programming (MILP) model was proposed to size BESSs in grid-connected MGs considering frequency stability constraints based on the discretised swing equation. In [28], a mixed-integer non-linear programming (MINLP) model was introduced for optimal sizing, siting, and setting of distributed energy resources (DERs) in MGs that employs a droop control scheme for voltage and frequency regulation. The proposed MINLP model was solved using the genetic algorithm due to the non-linearity of the problem. The authors in [29] introduced a heuristic approach to the sizing of off-grid MG components, including PV, wind, BESSs, and diesel generators that are operated based on the droop control scheme. In [30], a frequency-constrained approach for MG sizing was proposed, which modelled long- and short-term uncertainties using scenario analysis and distributionally robust chance constraint methods. The authors in [31] proposed a frequency-constrained planning framework for integrated electricity-heat MGs based on the virtual inertia estimation and distributionally robust optimisation methods. In [32], a planning model was developed for the optimal sizing of integrated power and gas systems, considering the frequency security requirements. The study in [33] proposed a BESS sizing methodology for off-grid MGs that incorporates a new advanced load-frequency control based on a droop control scheme for frequency regulation. In [34], an optimisation-oriented approach was proposed to size BESS in an off-grid MG on Flinders Island, Australia. The presented approach employed the grey wolf meta-heuristic method to solve the optimisation problem, whereas DigSilent PowerFactory software was used to simulate the frequency response of the MGs.

1.3. Research Gaps and Contributions

In summary, Table 1 compares the related research works and the proposed model in terms of MG configuration and application types, focus of the problem, consideration of frequency requirements, and key remarks. A review of the existing literature reveals that although the previously discussed papers have offered useful perspectives on incorporating RES into MG design and planning, only a limited number of studies addressed integration in heavy industries, such as mining located in remote areas. Moreover, in a mining setting, MGs manage a considerable, high-quality, and generally uninterrupted energy supply that frequently functions around the clock. This creates considerable challenges for the extensive incorporation of RES [35]. For example, wind and solar technologies can overproduce during peak generation hours, which creates financial losses due to the curtailment of excess energy. Although some of this energy can be stored in BESSs, the storage duration of current battery technologies is restricted, and increasing battery capacity can be economically unjustifiable. In addition, the decline in ore grades and the need to extract more material

Table 1: Comparison of related works

Ref.	Off-grid MG	Sizing and Planning	Frequency Constraints	Application	Remarks
[14, 15]	✓	✓	-	residential	Designing residential off-grid MGs in rural areas
[16, 17]	-	✓	-	residential	Sizing of grid-connected MGs to minimise costs and emissions
[18, 19]	✓	✓	-	mining	Heuristically sizing of off-grid MGs for mining applications
[20]	-	✓	-	mining	Sizing of grid-connected mining MGs comprising PV+biogas+BESS to minimise costs and emissions
[22]	-	✓	✓	-	Sizing BESS for frequency support of power systems
[23]	✓	-	✓	residential	Developing frequency-constrained energy management for off-grid MGs
[21, 24–26]	-	-	✓	-	Proposing frequency-constrained unit commitment and grid-connected MGs
[27, 33, 34]	✓	✓	✓	residential	Sizing of BESS for frequency support of both grid-connected and off-grid MGs
[28–30]	✓	✓	✓	residential	Proposing frequency-constrained DER sizing for off-grid and grid-connected MGs
[31, 32]	-	✓	✓	-	Frequency-constrained design of integrated electricity + heat and gas MGs
Proposed	✓	✓	✓	mining	Developing multi-objective frequency-constrained design of off-grid MGs for mining applications

exacerbate the demand for energy, as well as the limited suitable terrain for RES assets that may overlap with areas rich in mineral resources, creating additional obstacles to large-scale renewable integration [35].

Furthermore, the provision of PFR and inertia support for mining MGs remains underexplored in the literature. This presents a significant challenge for the integration of RES into the backbone energy systems of mines, particularly due to their remote locations and the use of variable loads, such as fast chargers or trolley systems in the future electrified mines [11].

To address these research gaps, this paper introduces a new frequency-constrained MG design framework for heavy industries, such as mining, with a high penetration of RES. The model is formulated as a multi-objective bi-level optimisation problem to determine the optimal capacities for solar and wind systems, BESS units, and fossil fuel backup generators to meet the MG demand, while ensuring that frequency stability requirements, such as rate of change of frequency (RoCoF), minimum/maximum frequency, and steady-state frequency, are maintained within acceptable limits during disturbances. In this framework, the upper-level (UL) problem minimises the total net present cost (NPC) of MG, mitigates GHG emissions, and improves system reliability considering both calendar and cycling degradation of BESSs. In the lower-level (LL) problem, the operation of the MG is simulated considering unit commitment, battery operation, and

frequency stability constraints. The non-dominated sorting genetic algorithm II (NSGA-II) [36, 37] is used to solve the UL multi-objective optimisation problem to determine DER capacities, which are evaluated by solving the LL problem, formulated as a MILP problem. This iterative process enables the assessments of objective functions and determining the trade-offs between them. Subsequently, fuzzy decision-making method is applied to the non-dominated solutions to obtain the final optimal plan. The key contributions of this study are summarised below.

- Unlike previous studies (e.g., [18–20]) that often overlook dynamic frequency constraints or treat them post-optimisation, this work proposes a novel multi-objective bi-level optimisation model for planning off-grid mining MGs. The model integrates wind, solar, BESSs, and fossil-fuel generators while explicitly incorporating PFR, inertia constraints, and battery degradation into the planning framework.

- Unlike existing works (e.g., [14, 15, 28–30]) that primarily focus on designing grid-connected or off-grid MGs for residential or general industrial applications, this study develops a tailored planning framework for mining MGs in remote areas. It addresses the integration of large-scale RES while maintaining frequency stability, considering the unique operational characteristics and reliability requirements of mining sites.

- Unlike conventional MG planning frameworks (e.g., [14–20]) that neglect the multi-functional role of BESSs, this work explicitly models their contribution to both energy balancing and dynamic frequency support. The results show that BESSs significantly reduce RES curtailment and always ensure compliance with frequency standards, demonstrating their critical role in improving both operational and economic performance.

- Unlike prior studies that often rely on hypothetical or average input data, this work employs a real-world case study of a remote underground mining MG in Australia. The model is validated using high-resolution (5-minute intervals) historical demand, site-specific RES generation, and realistic economic parameters.

The remainder of this paper is as follows. An overview of the proposed MG design framework is provided in Section 2. Section 3 provides an in-depth exploration of the problem formulation and the frequency control of the MG provided by the BESSs and fossil fuel generators. The linearisation procedure and the proposed solution methodology are described in Section 4. In Section 5, numerical results and discussions are provided, followed by conclusions and suggestions for further work in Section 6.

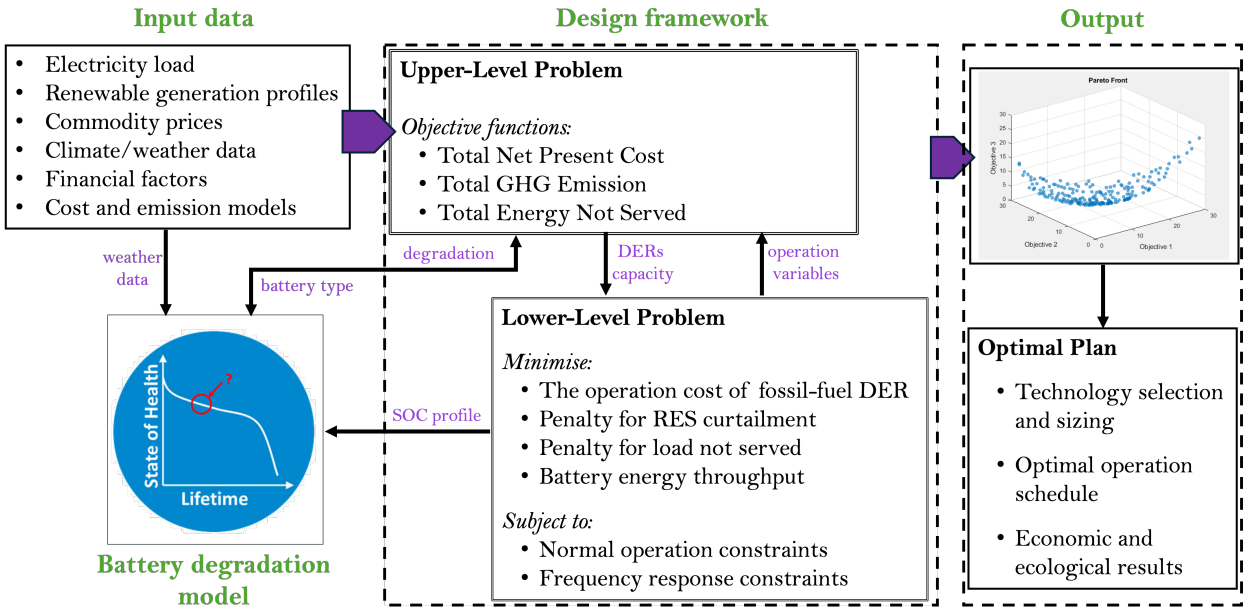

Figure 1: The structure of the proposed frequency-constrained MG design framework.

2. Model Overview

Figure 1 presents the high-level schematic of the proposed multi-objective bi-level architecture for MG design under frequency restrictions. As illustrated in the figure, the design framework uses input data such as RES production at the mine site, electricity load demand, cost and emission data, as well as financial parameters. Additionally, the design framework requires various technical input parameters, linked to each DER technology, especially the battery degradation model. In this work, the model developed by the National Renewable Energy Laboratory (NREL), that is, the Battery Lifetime Analysis and Simulation Toolsuite (BLAST), are used for the end-of-life analysis of the BESS [38].

Embedded within the design framework is a bi-level optimisation problem, which captures both the planning and operational aspects of MG design in a coordinated manner. The UL problem is formulated as a multi-objective optimisation that simultaneously minimises: (i) the NPC of the MG over its lifetime, (ii) GHG emissions, and (iii) the amount of ENS as the reliability index.

The UL problem determines the optimal capacities of various DERs, including PV, wind turbines, BESS, and back-up generators. These decisions are passed down as input parameters to the LL problem, which is formulated as a MILP. The LL problem simulates the detailed operation and scheduling of the MG over a representative time horizon.

The LL problem incorporates two major sets of constraints. The first set governs normal operational be-

haviour, including load balance equations, generator output limits, and battery charge/discharge restrictions. The second set of constraints enforces frequency response requirements, ensuring the MG can adequately respond to disturbances and maintain stability under various incidents, such as large load or generation fluctuations. These frequency-related operational considerations (key novelties of our work) address aspects often overlooked by most existing MG planning frameworks, which typically neglect frequency stability constraints or handle them with simplified metrics instead of detailed modelling.

The LL optimisation yields several key outputs, including:

- The dispatch schedule of backup generators,
- The amount of curtailed renewable energy (PV and wind),
- The unserved load during both normal and frequency-disturbance conditions,
- And the state-of-charge (SOC) profile of the BESS over time.

These outputs are used in the UL problem to evaluate the objective functions. Specifically, the SOC profile is used as an input to the BLAST model, which estimates BESS degradation and calculates its end-of-life. The estimated degradation is then incorporated into the NPC calculation in the UL problem, providing a more realistic cost estimation that accounts for battery replacement and salvage value during the MG lifetime.

The UL problem uses this feedback to update DER capacities and repeats the process iteratively, passing new decisions to the LL problem in each iteration. This iterative process between the UL and LL problems continues until a convergence criterion is met—either based on minimal changes in decision variables and objective values or upon reaching the maximum number of iterations.

The output of this design framework is the Pareto optimal solutions obtained based on the objectives specified earlier. These solutions are non-dominated MG designs that provide various capacity-sizing scenarios for DER technologies, giving decision-makers a range of options. However, for further analysis in this work, fuzzy min-max decision making algorithm is used to find the optimal plan among the Pareto solutions.

This hierarchical and integrated design approach ensures that the final MG design is technically feasible, economically optimal, and reliable by accounting for the complex interactions between planning decisions and operational requirements under both normal conditions and contingencies. Compared to the existing bi-level optimisation models in MG planning, our proposed approach introduces several methodological advances. It tightly integrates frequency response constraints within the operational layer and links battery

operational behaviour to long-term degradation modelling through BLAST. This holistic view enables more realistic planning decisions, particularly for applications such as mine electrification or off-grid MGs, where frequency stability and battery lifecycle costs are critical.

3. Problem Formulation

This section presents a detailed formulation of the proposed MG design model. First, the frequency control of the MG provided by BESSs and fossil fuel generators is introduced. Subsequently, a mathematical formulation of the UL problem is presented, along with the cost and emission models of the MG components. Next, a mathematical formulation of the MG scheduling problem is provided at the lower level, considering the constraints associated with frequency control, which is managed by the BESS and fossil fuel generators.

3.1. Frequency Control of BESS Supported MG

The frequency dynamics of an off-grid MG with the contribution of synchronous generators and BESS for the PFR can typically be approximated using the first-order swing equation [30, 39]:

$$\frac{d\Delta f(\tau)}{d\tau} = \frac{1}{2H}\left(\Delta PG + \Delta PB - \Delta PL^{max}\right) \tag{1}$$

where $\Delta f(\tau)$ is the frequency deviation following a power disturbance ΔPL^{max} while ΔPG and ΔPB represent the PFR provided by diesel generators and BESSs, respectively. In addition, H is the aggregated inertia of the system contributed by the diesel generators. It should be noted that because an off-grid MG dominated by power electronic resources is a typical low-inertia system, the load damping level is low and is therefore neglected in Eq. (1).

According to this equation, in the absence of BESS support during a contingency, the frequency deviation in the first few seconds (Δt_1, 0-5s) can only be limited by the inertial response of the diesel generators in off-grid MGs. As soon as the governor deadband is passed, the PFR activates the primary reserve to restore the frequency to a quasi-steady-state value. The PFR typically lasts for 5 to 25 seconds (Δt_2). BESS, due to its rapid response time and ability to ramp fully in a timeframe of tens to hundreds of milliseconds, acts as an effective energy source for reducing power imbalances [22, 40]. Hence, when a contingency occurs, BESS will charge/discharge immediately based on its additional power available to reduce the power imbalance in the system. This process is expressed by

$$\Delta PB = \begin{cases} PB^{bt,max} - PB^{dis} + PB^{ch} & ;\Delta PL^{max} \geq 0 \\ -PB^{bt,max} + PB^{ch} - PB^{dis} & ;\Delta PL^{max} \leq 0 \end{cases} \tag{2}$$

$$PB^{ch,max} \leq PB^{bt,max} \leq PB^{dis,max} \tag{3}$$

$$\Delta PL = \Delta PL^{max} - \Delta PB \tag{4}$$

where $PB^{bt,max}$ represents the maximum required charge/discharge power of BESS while $PB^{dis,max}$ and $PB^{ch,max}$ are, respectively, the maximum allowable power of BESS that can be immediately injected into or absorbed from the system to compensate for the power imbalance. In addition, PB^{dis} and PB^{ch} are the discharge and charge power of the BESS before the contingency event, respectively. Therefore, the power imbalance remains constant during the inertia response period (Δt_1), considering that the BESS power injection/absorption is constant during the transient period. Once the governor's deadband is surpassed, diesel generators initiate the PFR at a steady rate. During the PFR period (Δt_2), the power imbalance decreases linearly until it reaches zero, bringing the system to a quasi-steady state.

Moreover, after inertia and PFR, the secondary frequency response (SFR) will commence to restore the frequency to the nominal value. In this phase, ΔPB will return linearly to 0, so that the batteries will not cause a sudden power imbalance during the SFR time interval (Δt_3, normally 5 minutes). Hence, to ensure that the BESS has sufficient energy to provide power support following a contingency, the amount of energy ΔE that the BESS must be able to charge/discharge to help deal with the post-contingency frequency deviation is [21, 22]:

$$\Delta E = \Delta PB^{ch/dis,max} \left(\Delta t_1 + \Delta t_2 + 0.5\Delta t_3\right) \tag{5}$$

3.2. UL Problem

The first objective function of the UL problem is to minimise the total NPC over the life of the MG, expressed as:

$$NPC = \sum_{i \in \Psi} \left(C_i^C + C_i^O + C_i^R - C_i^S\right) \tag{6}$$

where $\Psi = \{PV, WT, BT, DG\}$ is the set of MG energy sources consisting of solar PV, wind turbine, lithium-ion BESS, and diesel generators (DGs). In this equation, $C_i^{[.]}$ denotes the net present value of the total cost associated with DER i and the superscripts C, O, R, and S represent capital, operation and maintenance, replacement, and salvage, respectively. In this regard, the capital costs of DER technologies can be expressed as:

$$C_i^C = c_i^I P_i \;\; \forall i \in \{PV, WT\} \tag{7}$$

$$C_{DG}^C = \sum_{g \in G} c_g^I P_g^{max} \tag{8}$$

$$C_{BT}^C = c_{BT}^p P_{BT} + c_{BT}^e E_{BT} \tag{9}$$

where (7) calculates the capital costs of the solar and wind units based on their installed power capacity, while (8) represents the capital cost of diesel generators. The capital cost of BESS includes two terms related to energy capacity and power, as shown in (9).

Generally, the operation and maintenance cost of RES, i.e., solar PV and wind systems, as well as BESS are calculated as a portion of its annualised capital cost [41]. Hence, the present value of the operation cost for these components can be expressed as:

$$C_i^O = \sum_{y=1}^{L_{mg}} \frac{c_i^O P_i}{(1+ir)^y} \;\; \forall i \in \{PV, WT, BT\} \tag{10}$$

The operation cost of diesel generators includes maintenance and fuel consumption costs as:

$$C_{DG}^O = \sum_{y=1}^{L_{mg}} \sum_{g \in G} \frac{P_g^{max} c_g^M + E_{g,yr} c_g^F}{(1+ir)^y} \tag{11}$$

where $E_{g,yr}$ is calculated by solving the LL problem.

Moreover, during the life of the MG, we may need to replace several assets. This occurs for specific components of renewable units, such as inverters and PV modules, as well as wind turbine nacelles and rotors. Hence, the present value of the replacement cost of solar PV (C_{PV}^R) due to regular inverter replacement and PV modules failures, and wind systems (C_{WT}^R) due to rotor and nacelle replacement, can be expressed as below.

$$C_{PV}^R = \sum_{y=1}^{\lfloor \frac{L_{mg}}{L_{\mathtt{in}}} \rfloor} \frac{c_{\mathtt{in}}^I P_{PV}}{(1+ir)^{yL_{\mathtt{in}}}} + \sum_{y=W_{\mathtt{md}}+1}^{L_{mg}} \frac{f_{PV} c_{\mathtt{md}}^I P_{PV}}{(1+ir)^y} \tag{12}$$

$$C^R_{WT} = \sum_{y=1}^{\lfloor \frac{L_{mg}}{L_{\mathtt{rt}}} \rfloor} \frac{c^I_{\mathtt{rt}} P_{WT}}{(1+ir)^{yL_{\mathtt{rt}}}} + \sum_{y=1}^{\lfloor \frac{L_{mg}}{L_{\mathtt{nc}}} \rfloor} \frac{c^I_{\mathtt{nc}} P_{WT}}{(1+ir)^{yL_{\mathtt{nc}}}} \tag{13}$$

Furthermore, the replacement cost for BESSs consists of two parts: (1) power conversion system and (2) battery modules and cells. The replacement cost of the power conversion system is similar to that of the inverter in a PV system. However, the cost of replacing battery modules and cells is related to the rate of degradation of battery capacity as a result of cycling and calendar ageing. Thus, the present value of BESS replacement cost (C^R_{BT}) is as follows:

$$C^R_{BT} = \sum_{y=1}^{\lfloor \frac{L_{mg}}{L_{\mathtt{pc}}} \rfloor} \frac{c^I_{\mathtt{pc}} P_{BT}}{(1+ir)^{yL_{\mathtt{pc}}}} + \sum_{y=1}^{\lfloor \frac{L_{mg}}{L_{\mathtt{ec}}} \rfloor} \frac{c^I_{\mathtt{ec}} E_{BT}}{(1+ir)^{yL_{\mathtt{ec}}}} \tag{14}$$

In the above equation, $L_{\mathtt{ec}}$ represents the life of the battery units, which can be calculated based on calendar and cycling ageing. In this study, we use the BLAST-Lite library to calculate battery degradation [38]. According to this package, $L_{\mathtt{ec}}$ can be expressed as

$$L_{\mathtt{ec}} = \frac{1 - EoL}{e_{loss,yr}} \tag{15}$$

$$e_{loss,yr} = f_{BLAST}(SOC, Temp, BT_{Type}) \tag{16}$$

where $e_{loss,yr}$ represents the percentage of energy losses per year of the battery that is calculated based on the SOC of the battery, temperature, and battery type using the BLAST-Lite package [38].

It should be noted that these replacement costs assume that the lifespan of other assets within the solar PV and wind systems exceeds that of the MG. Furthermore, without loss of generality, the lifetimes of diesel generators are assumed to be longer than L_{mg}; hence, there is no replacement cost. However, the replacement cost model developed can be easily adjusted for scenarios in which this assumption does not hold.

The last term in the NPC is the salvage value of the MG components at the end of the project lifetime that can generally be expressed for DERs as

$$C^S_i = \sum_{k \in K_i} C_{i,k} \left(1 - \frac{2}{L_{k,i}}\right)^{L_{mg}} \frac{1}{(1+ir)^{L_{mg}}} \tag{17}$$

where $C_{i,k}$ represents the capital cost of the component k of DER i.

The other objective functions of the UL problem are minimisation of total GHG emissions (EM) and

total energy not served (ENS) as a reliability index, as follows.

$$EM = \sum_{e \in E} \pi_e \sum_{t \in T} \sum_{g \in G} em_g P_{g,t,e} \Delta T \tag{18}$$

$$ENS = \sum_{e \in E} \pi_e \sum_{t \in T} \left(P^{ns}_{t,e} \Delta T + \Delta P^{ns}_{t,e} \Delta T' \right) \tag{19}$$

Note that $P_{g,t,e}$, $P^{ns}_{t,e}$, and $\Delta P^{ns}_{t,e}$ are the decision variables for the LL problem and the GHG emissions in (18) are calculated considering that RES and BESS do not produce any operational emissions. Note that ENS should be less than a certain value in the MG design [42] to meet reliability requirements. Hence, in this study, (19) is converted to a constraint as follows:

$$\sum_{e \in E} \pi_e \sum_{t \in T} \left(P^{ns}_{t,e} \Delta T + \Delta P^{ns}_{t,e} \Delta T' \right) \leq \overline{ENS} \tag{20}$$

The UL problem is subject to the following constraints with respect to the maximum installed capacity of RES and BESSs (21), DGs (22) and the relationship between BESS power and energy capacities (23).

$$0 \leq P_i \leq P^{max}_i; \;\; \forall i \in \{PV, WT, BT\} \tag{21}$$

$$0 \leq \sum_{g \in G} P^{max}_g \leq P^{max}_{DG} \tag{22}$$

$$C^{min}_{rate} E_{BT} \leq P_{BT} \leq C^{max}_{rate} E_{BT} \tag{23}$$

3.3. LL Problem

The LL problem simulates the frequency-constrained scheduling of MG using the DER capacities determined by the UL problem. The objective function of the LL problem is to minimise the total scheduling cost expressed as:

$$\begin{aligned} OF = \sum_{e \in E} \pi_e \sum_{t \in T} \Bigg(& \sum_{g \in G} (a_g P_{g,t,e} + b_g u_{g,t,e} + c^r_g R_{g,t,e}) \Delta T \\ & + (\Gamma P^{RES,cu}_{t,e} + \Lambda P^{ns}_{t,e}) \Delta T + \Upsilon \Delta P^{ns}_{t,e} \Delta T' \\ & + c^d_{BT} (P^{ch}_{t,e} + P^{dis}_{t,e}) \Delta T \Bigg) \end{aligned} \tag{24}$$

where the first term calculates the total fuel cost of the DG and the cost of PFR. The second, third, and fourth terms introduce penalty terms designed to ensure that the optimisation problem minimises both RES curtailment and load shedding to the greatest extent possible, both before and during the PFR. The

last term represents the cost of energy throughput of BESS to minimise the degradation of the battery by avoiding unnecessary charging and discharging. It is worth noting that we ignore the start-up and shutdown costs in the LL objective function, as in mining applications only fast-response diesel generators are used. These units can start up or shut down in under a minute, and the associated costs are negligible compared to their operational costs [43].

This objective function is bounded by a set of constraints, as explained in the following subsections.

3.3.1. Normal operation

1) Supply-demand balance: This constraint ensures that demand and supply from multiple sources are matched at any time.

$$\sum_{g \in G} P_{g,t,e} + P_{t,e}^{WT} + P_{t,e}^{PV} + P_{t,e}^{dis} - P_{t,e}^{ch} - P_{t,e}^{RES,cu} + P_{t,e}^{ns} = Pd_{t,e} \; ; \forall t \in T, e \in E \tag{25}$$

2) Renewable energy production: The power production of the RES is calculated based on the predicted normalised value and the installed capacity as follows:

$$P_{t,e}^{PV} = P_{PV} \overline{P_{t,e}^{pv}} \; ; \forall t \in T, e \in E \tag{26}$$

$$P_{t,e}^{WT} = P_{WT} \overline{P_{t,e}^{wt}} \; ; \forall t \in T, e \in E \tag{27}$$

3) Diesel generator constraints: The constraints associated with the operation of DGs are as follows.

$$P_g^{min} u_{g,t,e} \leq P_{g,t,e} \leq P_g^{max} u_{g,t,e} \; ; \forall g \in G, t \in T, e \in E \tag{28}$$

$$-RD_g \Delta T \leq P_{g,t,e} - P_{g,t-1,e} \leq RU_g \Delta T \; ; \forall g \in G, t \in T, e \in E \tag{29}$$

$$T_{g,t,e}^{ON} \geq UT_g \left(u_{g,t,e} - u_{g,t-1,e} \right) \Delta T \; ; \forall g \in G, t \in T, e \in E \tag{30}$$

$$T_{g,t,e}^{OFF} \geq DT_g \left(u_{g,t-1,e} - u_{g,t,e} \right) \Delta T \; ; \forall g \in G, t \in T, e \in E \tag{31}$$

where (28) limits the power generation of each generator while (29) enforces ramp-up and ramp-down constraints. Additionally, (30) and (31) apply the minimum up and down times of DGs.

4) BESS constraints: The operation of BESSs requires a set of constraints as follows.

$$0 \leq P_{t,e}^{ch} \leq P_{BT} Z_{t,e} \; ; \forall t \in T, e \in E \tag{32}$$

$$0 \leq P_{t,e}^{dis} \leq P_{BT}(1 - Z_{t,e}) \; ; \forall t \in T, e \in E \tag{33}$$

$$SoE_{t,e} = SoE_{t-1,e} + \left(\eta^{ch} P_{t,e}^{ch} - \frac{P_{t,e}^{dis}}{\eta^{dis}} \right) \Delta T \; ; \forall t \in T, e \in E \tag{34}$$

$$SoE^{min} E_{BT} \leq SoE_{t,e} \leq SoE^{max} E_{BT} \; ; \forall t \in T, e \in E \tag{35}$$

$$SoE_{0,e} = SoE_{T,e} \; ; \forall e \in E \tag{36}$$

where the charge and discharge powers of the BESSs is limited by equations (32) and (33). Equation (34) determines the state of energy (SoE) of BESSs at each time interval, subject to the constraints outlined in (35). Furthermore, the constraint (36) guarantees that the starting SoE is equal to the end-of-day SoE.

3.3.2. Frequency control constraints

During the short-term transient period, the MG frequency control constraints are primarily centred on the RoCoF, quasi-steady-state frequency, and frequency nadir/overshoot. These parameters are integral to maintaining system security through dynamic frequency regulation and hence preventing system collapse.

1) System-wide power imbalance: As mentioned earlier, following a contingency event (e.g., load drop/increase or loss of a generation unit) at time t, the BESS immediately injects/absorbs power at full capacity P_{BT} to compensate for the power imbalance. The power change in the BESS is

$$\Delta PB_{t,e} = P_{t,e}^{bt,max} - P_{t,e}^{dis} + P_{t,e}^{ch} \; ; \forall t \in T, e \in E \tag{37}$$

$$-P_{BT} \leq P_{t,e}^{bt,max} \leq P_{BT} \; ; \forall t \in T, e \in E \tag{38}$$

Therefore, the power imbalance of the system is reduced to

$$\Delta PL_{t,e} = \Delta PL_{t,e}^{max} - \Delta PB_{t,e} \; ; \forall t \in T, e \in E \tag{39}$$

Note that this equation should be rewritten as follows to consider under-frequency load shedding (UFLS) when the available resources cannot manage the frequency drop and the UFLS relays take action to maintain the frequency within the standard range.

$$\Delta PL_{t,e} = \Delta PL_{t,e}^{max} - \Delta PB_{t,e} - \Delta P_{t,e}^{ns} \; ; \forall t \in T, e \in E \tag{40}$$

$$0 \leq \Delta P_{t,e}^{ns} \leq \Delta PL_{t,e}^{max} \; ; \forall t \in T, e \in E \tag{41}$$

2) RoCoF limit: As described by (1), the highest RoCoF ($\frac{d\Delta f(\tau)}{d\tau}$) occurs at $\tau = 0$, in the absence of PFR measures by synchronous generators, which should be constrained $\forall t \in T, e \in E$, as noted in [30]:

$$\left.\frac{d\Delta f(\tau)}{d\tau}\right|_{\tau=0} = \frac{|\Delta PL_{t,e}|}{2H_{t,e}} \leq RoCoF^{max} \tag{42}$$

where the inertia of the system $H_{t,e}$ is calculated as:

$$H_{t,e} = \frac{\sum_{g \in G} H_g P_g^{max} u_{g,t,e}}{f^0} \; ; \forall t \in T, e \in E \tag{43}$$

By substituting (43) into (42) and rearranging the equation, the RoCoF constraint can be expressed as [21, 44]:

$$\frac{\sum_{g \in G} H_g P_g^{max} u_{g,t,e}}{f^0} \geq \frac{|\Delta PL_{t,e}|}{2RoCoF^{max}} \; ; \forall t \in T, e \in E \tag{44}$$

3) Frequency nadir/overshoot limit: The frequency nadir refers to the lowest point of frequency observed during the transient phase prior to the commencement of frequency recovery. The frequency nadir occurs due to a sudden increase in load or loss of generation and must be greater than a pre-specified limit to warrant a preventive/corrective action. In contrast, frequency overshoot refers to the peak frequency attained during the transient phase as a result of an abrupt reduction in load or an increase in supply, which must remain below a predetermined threshold. In this regard, [45] proved that the following conditions are sufficient to ensure that these frequencies remain within the specified limits.

$$R_{g,t,e} \leq 2v_g \frac{H_{t,e}\left(\overline{\Delta f} - f^{db}\right)}{|\Delta PL_{t,e}|} \; ; \forall g \in G, t \in T, e \in E \tag{45}$$

$$\sum_{g \in G} R_{g,t,e} \geq |\Delta PL_{t,e}| \; ; \forall t \in T, e \in E \tag{46}$$

where $\overline{\Delta f}$ is the maximum acceptable frequency deviation, calculated as $\overline{\Delta f} = f^0 - f^{min}$ or $\overline{\Delta f} = f^{max} - f^0$. Constraint (45) ensures that the primary reserve of each generator is delivered by the time the frequency nadir/overshoot occurs. Constraint (46) ensures that the synchronous units currently operating online offer adequate primary reserve to address a power imbalance of $\Delta PL_{t,e}$.

4) Primary reserve limits of the synchronous units: The primary reserve constraints are as follows:

$$0 \leq R_{g,t,e} \leq R_g^{max} \; ; \forall g \in G, t \in T, e \in E \tag{47}$$

$$P_g^{min} u_{g,t,e} \leq P_{g,t,e} + R_{g,t,e} \leq P_g^{max} u_{g,t,e} \; ; \forall g \in G, t \in T, e \in E \tag{48}$$

Constraint (47) sets the minimum and maximum limits for the primary reserve provided by each generator. Meanwhile, constraint (48) ensures that the primary reserve allocated to each generator does not exceed the available spinning headroom, which is the portion of capacity that can contribute to the PFR.

5) Contingency SoE Limits of the BESS: The SoE constraint during the contingency is

$$0 \leq SoE_{t,e} - \Delta E_{t,e} \leq SoE^{max} E_{BT} \; ; \forall t \in T, e \in E \tag{49}$$

Constraint (49) ensures that the SoE of each BESS unit is sufficient to manage frequency disturbances during the transient period. As contingency events are generally rare in any power system, the minimum SoE during this period can be set to zero. After the system stabilises, the BESS must gradually return to its original setpoint as SFR actions are fully deployed. The energy $\Delta E_{t,e}$ that BESS must discharge/charge to address post-contingency frequency deviation is given by

$$\Delta E_{t,e} = P_{t,e}^{bt,max} \left(\Delta t_1 + \Delta t_2 + 0.5 \Delta t_3 \right) \; ; \forall t \in T, e \in E \tag{50}$$

where Δt_1, Δt_2, and Δt_3 are typically 5 sec, 25 sec, and 5 min, respectively.

4. Solution Methodology

As mentioned in Section 2 and shown in the formulation, the proposed MG design approach is a multi-objective bi-level optimisation problem with non-linearity in both UL and LL problems. Although the non-linearity in the LL problem can be mathematically linearised, as will be explained in this section, the UL nonlinear terms cannot be easily linearised. The reason is that these non-linearities are mainly associated with calculating replacement cost and salvage value of the BESS, which is a non-linear function of the BESS life. Furthermore, the lifespan of the BESS is determined by evaluating its degradation, which exhibits a non-linear relationship with its usage. Hence, this paper proposes a solution methodology that uses the BLAST-Lite package for calculating the BESS degradation and dealing with UL non-linearities, linearising the LL problem to form an MILP to be solved by commercial solvers, and applying the evolutionary algorithm NSGA-II for solving the UL problem.

The non-linearity of the LL problem arises from constraints (44)-(46). Because $\Delta PL_{t,e}^{max}$ is a parameter, we can divide the LL problem into two subproblems: one for $\Delta PL_{t,e}^{max} \geq 0$ (load increase or supply decrease) and the other for $\Delta PL_{t,e}^{max} \leq 0$ (load decrease or supply increase). However, without loss of generality, only the $\Delta PL_{t,e}^{max} \geq 0$ case is considered, because generation outages and load increases have a greater impact on the system and are more difficult to resolve. Therefore, $|\Delta PL_{t,e}|$ can be replaced with $\Delta PL_{t,e}$ in (44)-(46). This will resolve the non-linearity in (44) and (46); however, constraint (45) remains non-linear due to the product of two continuous variables $R_{g,t,e}$ and $\Delta PL_{t,e}$. To linearise this term, we first rewrite it as follows using (37) and (40)

$$\begin{aligned} R_{g,t,e}\left(\Delta PL_{t,e}^{max} - \left(P_{t,e}^{bt,max} - P_{t,e}^{dis} + P_{t,e}^{ch}\right) - \Delta P_{t,e}^{ns}\right) \\ \leq 2v_g H_{t,e}\left(f^0 - f^{min} - f^{db}\right) \; ; \forall g \in G, t \in T, e \in E \end{aligned} \tag{51}$$

Now we have four non-linear terms as $R_{g,t,e}P_{t,e}^{bt,max}$, $R_{g,t,e}P_{t,e}^{dis}$, $R_{g,t,e}P_{t,e}^{ch}$, and $R_{g,t,e}\Delta P_{t,e}^{ns}$. Since all variables are bounded, we can use McCormick's envelopes for linearisation as follows [21, 46].

$$\begin{aligned} A_{g,t,e} &= R_{g,t,e}P_{t,e}^{bt,max} \\ B_{g,t,e} &= R_{g,t,e}P_{t,e}^{dis} \\ C_{g,t,e} &= R_{g,t,e}P_{t,e}^{ch} \\ D_{g,t,e} &= R_{g,t,e}\Delta P_{t,e}^{ns} \end{aligned} \quad ; \forall g \in G, t \in T, e \in E \tag{52}$$

$$R_{g,t,e}\Delta PL_{t,e}^{max} - \left(A_{g,t,e} - B_{g,t,e} + C_{g,t,e}\right) - D_{g,t,e} \leq 2v_g H_{t,e}\left(f^0 - f^{min} - f^{db}\right) \; ; \forall g \in G, t \in T, e \in E \tag{53}$$

$$A_{g,t,e}, B_{g,t,e}, C_{g,t,e}, D_{g,t,e} \geq 0 \; ; \forall g \in G, t \in T, e \in E \tag{54}$$

$$-A_{g,t,e} + P_{BT} R_{g,t,e} \geq 0 \; ; \forall g \in G, t \in T, e \in E \tag{55}$$

$$-A_{g,t,e} + R_g^{max} P_{t,e}^{bt,max} \geq 0 \; ; \forall g \in G, t \in T, e \in E \tag{56}$$

$$A_{g,b,t} + R_g^{max} P_b^{batt} - R_g^{max} P_{t,e}^{bt,max} - P_{BT} R_{g,t,e} \geq 0 \; ; \forall g \in G, t \in T, e \in E \tag{57}$$

$$-B_{g,t,e} + P_{BT} R_{g,t,e} \geq 0 \; ; \forall g \in G, t \in T, e \in E \tag{58}$$

$$-B_{g,t,e} + R_g^{max} P_{t,e}^{dis} \geq 0 \; ; \forall g \in G, t \in T, e \in E \tag{59}$$

$$B_{g,t,e} + R_g^{max} P_{BT} - R_g^{max} P_{t,e}^{dis} - P_{BT} R_{g,t,e} \geq 0 \; ; \forall g \in G, t \in T, e \in E \tag{60}$$

$$-C_{g,t,e} + P_{BT} R_{g,t,e} \geq 0 \; ; \forall g \in G, t \in T, e \in E \tag{61}$$

$$-C_{g,t,e} + R_g^{max} P_{t,e}^{ch} \geq 0 \; ; \forall g \in G, t \in T, e \in E \tag{62}$$

$$C_{g,t,e} + R_g^{max} P_{BT} - R_g^{max} P_{t,e}^{ch} - P_{BT} R_{g,t,e} \geq 0 \; ; \forall g \in G, t \in T, e \in E \tag{63}$$

$$-D_{g,t,e} + \Delta PL_{t,e}^{max} R_{g,t,e} \geq 0 \; ; \forall g \in G, t \in T, e \in E \tag{64}$$

$$-D_{g,t,e} + R_g^{max} \Delta P_{t,e}^{ns} \geq 0 \; ; \forall g \in G, t \in T, e \in E \tag{65}$$

$$D_{g,t,e} + R_g^{max} \Delta PL_{t,e}^{max} - R_g^{max} \Delta P_{t,e}^{ns} - \Delta PL_{t,e}^{max} R_{g,t,e} \geq 0 \; ; \forall g \in G, t \in T, e \in E \tag{66}$$

Note that when assuming $\Delta PL_{t,e}^{max} \geq 0$, equation (38) transforms into

$$0 \leq P_{t,e}^{bt,max} \leq P_{BT} \; ; \forall t \in T, e \in E \tag{67}$$

Therefore, the proposed LL problem can be expressed as the following MILP optimisation problem:

$$\min (24) \tag{68}$$

s.t.

$$(25) - (37), (40), (41), (44), (46) - (50), (53) - (67) \tag{69}$$

where constraints (25)-(36) express the normal operation of the MG, (37),(40),(41),(67) calculate the power imbalance due to an incident, (44) limits the RoCoF, (46)-(50) express the steady-state frequency requirement, and (53)-(66) present the linearised constraints for modelling the frequency nadir.

As previously mentioned, the NSGA-II algorithm with the help of a MILP solver for LL problem is employed to solve the proposed multi-objective bi-level frequency-constrained MG design problem. The pseudocode for the solution methodology is illustrated in Algorithm 1, which outlines the key steps of the algorithm used to solve the proposed optimisation problem. As illustrated, initially, NSGA-II randomly generates a population of candidate MG design by assigning values to the decision variables representing the capacities of various DERs. Each of these design plans is then passed to the LL problem as input to simulate the MG's operational behaviour under both normal and contingency conditions. The LL problem yields operational variables such as generator dispatch ($P_{g,t,e}$), load not served ($P^{ns}_{t,e}$), state of energy of the BESS ($SoE_{t,e}$), and frequency-related unserved power ($\Delta P^{ns}_{t,e}$).

These outputs are then passed to the UL problem to evaluate the objective functions, including NPC and GHG emissions. If a BESS is included in the design, its SOC is computed using $SOC_{t,e} = SoE_{t,e}/E_{BT}$ and passed to the BLAST model to estimate battery degradation, which is then used in the UL problem to refine the NPC calculation, ensuring a more realistic economic evaluation. Additionally, if the total unserved energy exceeds the specified threshold, the objective functions are penalised to discourage such solutions and effectively remove them from the feasible solution space. Once all individuals are evaluated, NSGA-II ranks the solutions based on non-dominance and crowding distance and applies genetic operations such as crossover and mutation to generate a new population. This process is repeated iteratively until the termination criterion—defined by the maximum number of iterations—is met. The final output of this procedure is a Pareto-optimal set of MG planning solutions that balance economic, environmental, and reliability objectives.

Algorithm 1 Proposed Solution Methodology for Frequency Constrained MG Design Problem

Input: Data associated with load demand, RES profiles, contingency, cost and emission parameters

Output: Pareto optimal solutions

Generate the initial population considering (21)-(23)

while *termination criteria are not satisfied* **do**

  for *each individual in population* **do**

    Solve LL problem (68)-(69)

    Determine $P_{g,t,e}$, $P^{ns}_{t,e}$, $SoE_{t,e}$, and $\Delta P^{ns}_{t,e}$

    if $E_{BT} \neq 0$ **then**

      Calculate $SOC_{t,e} = SoE_{t,e}/E_{BT}$

      Run BLAST-Lite package to calculate $e_{loss,yr}$ using (16)

    end

    Calculate UL objective functions NPC and EM (6) and (18)

    Check ENS limits (20) and penalise fitness functions accordingly

  end

  Sort solutions based on non-dominancy ranks

  Choose parents based on non-dominancy ranks and crowding distances

  Generate new population of solutions by crossover and mutation of parents

end

The computational complexity of the proposed solution methodology arises from the interaction between the evolutionary algorithm NSGA-II in the UL problem and the MILP solver in the LL problem. Each candidate solution in the population requires MILP solutions to evaluate its feasibility and fitness. Thus, the time complexity of the framework is a function of $n_{Gen} n_{pop} T_{\text{LL}}$, where n_{Gen} is the number of generations, n_{pop} is the population size, and T_{LL} is the average time required to solve the MILP in the LL problem. While NSGA-II is efficient in handling multi-objective optimisation problems, the bottleneck in computational time is typically the MILP solver, particularly when the problem size increases.

To reduce computational burden, the following strategies were implemented:

- **Representative Days:** Instead of considering all operational days, representative days were selected to capture the variability in demand and renewable generation, significantly reducing the size of the problem.
- **MIP Gap:** A tolerance was set for the MILP solver's relative gap, ensuring near-optimal solutions

while reducing computation time.

- **Time Limit:** A maximum computation time was imposed on the MILP solver, trading exact solutions for feasible ones within practical limits.

5. Simulation Case Study

This section presents the results of the proposed frequency-constrained MG design framework for a real-world case study of an off-grid underground mine in Australia. The mine is located in a remote area with significant potential for solar and wind energy, showing capacity factors of approximately 43% for wind and 28% for solar, as depicted by the normalised production duration curves in Figure 2. The mine electrical load exhibits a consistent 24/7 pattern, with peak and average values of 11.75 MW and 9.75 MW, respectively, and a total annual energy demand of 87.9 GWh. This high inflexibility necessitates a nearly constant power supply, which presents significant financial challenges in the development of a (near) zero-emission MG, as demonstrated in this section. To address the extensive computational time involved in solving the LL problem for an entire year, we employ an approximation method using five representative days to capture the annual power generation from wind and solar units, along with load profiles and ambient temperature data. These representative days, identified using the scaled K-medoids clustering technique, each consist of 288 5-minute intervals, ensuring a tractable optimisation problem.

This method is applied using various random seeds to produce representative days that closely resemble the original dataset in terms of key characteristics—such as peak load, annual energy demand, capacity factors (CF), and maximum normalised output for PV and wind, as well as temperature extremes and averages. Traditional clustering methods, such as K-means and fuzzy clustering, tend to yield centroid values that often fail to reflect critical operational extremes. As shown in Table 2, the scaled K-medoids method stands out by exactly capturing the peak load (11.79 MW) and maximum temperature (41.8°C), which are crucial parameters in mine MG planning—particularly for sizing generation and storage systems and for assessing battery degradation under thermal stress.

Although the scaled method slightly overestimates annual energy demand and capacity factors (e.g., 87.9 GWh vs. 84.7 GWh and 30% PV CF vs. 28%), this introduces a conservative bias in generation availability assumptions that may lead to slightly undersized generation capacity. More importantly, capturing peak demand accurately is critical in planning for reliable power supply in mining operations. Additionally, unlike other clustering methods that underestimate maximum ambient temperatures (e.g., 29–33°C vs. 41.8°C), the scaled method preserves thermal extremes. Although battery systems typically employ active

or passive cooling to maintain internal temperatures, high ambient conditions still increase auxiliary loads such as HVAC consumption, affecting overall system efficiency and battery cycling. By retaining these extremes, the model adopts a conservative and robust approach that may overstate degradation and cost impacts—ensuring that the system is resilient under harsh conditions, while actual performance in practice may exceed the model's estimates.

Table 2: Comparison of clustering methods with real data

		Real data	Fuzzy clustering	K-means	Orig. K-medoids	Scl. K-medoids
Load	Peak (MW)	11.79	10.43	10.47	11.30	11.79
	Annual (GWh)	84.7	87.0	84.7	86.9	87.9
PV	CF (%)	28	28	28	28	29
	max	1	0.88	0.92	0.99	1
Wind	CF (%)	43	43	43	44	44
	max	1	0.71	0.84	0.96	1
Temp.	max (°C)	41.8	33.26	29.12	28.9	41.8
	Avg (°C)	17.1	17.08	17.08	17.5	23.7

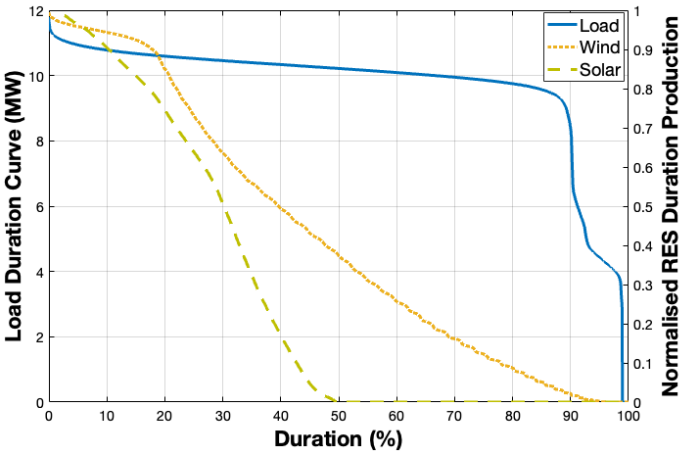

Figure 2: Electricity load duration curve and normalised potential RES production duration for the mine

Simulation studies require a variety of input data, including cost and emission parameters, as well as technical specifications of the energy sources. Detailed cost and emission data are available in [47], with a summary presented in Table 3. DGs were chosen as the fossil fuel source because of the absence of a natural gas pipeline at that location. The MG is assumed to operate for 25 years, with a compound interest rate of 3.1%. The maximum capacities for wind, PV, and BESS units are established at three times the peak demand (35 MW), and up to 6 DG units, each with a maximum capacity of 5 MW. Additionally, DGs are assumed to be identical, with an inertia constant of 4 seconds, a maximum governor ramp rate of 0.15

pu/sec, and a maximum primary reserve of 0.4 pu.

In this study, since we focus on off-grid mining microgrids, which are typically self-governed and not subject to uniform external regulatory requirements, we adopt representative industry standards to ensure consistency, technical rigour, and relevance. Specifically, the system is designed to comply with IEEE Std 1547-2018 and the Western Australia Electricity Market standards, which specify a maximum allowable RoCoF of 0.5 Hz/s [48, 49]. For maximum frequency deviations, we refer to the Frequency Operating Standards of Western Australia and the Australian National Electricity Market (NEM) for islands, which define a normal operating frequency range of 49.5–50.5 Hz [50, 51].

Accordingly, the power disturbance considered here is assumed to be a sudden increase in load by 15% of the total load [30]. The frequency requirements are set as follows: nominal frequency $f^0 = 50$ Hz, maximum allowable RoCoF $RoCoF^{max} = 0.5$ Hz/s, minimum allowable frequency $f^{min} = 49.5$ Hz and governor deadband $f^{db} = 20$ mHz [21]. To ensure maximum reliability, all Pareto-optimal solutions must achieve zero ENS, i.e., $\overline{ENS} = 0$. The modelling assumptions—including frequency requirements, cost and emission parameters, demand profiles, and renewable energy resource data—are based on typical operational conditions of off-grid mining MGs. These parameters were selected to strike a balance between realistic representation and computational tractability.

Table 3: Summary of the main cost and emission assumptions in the simulation study

	Solar PV	Wind System	Lithium-ion (4 hours, 0.25C)	Diesel Generator
Capital Cost ($/kW)	1800	2200	2644	1200
Fixed O&M ($/kW-yr)	45	60	7.57	52.5
Fuel Cost ($/kWh)	-	-	-	0.17
Life Time (Years)	25	25	12	25
Emission (kg CO_2-e/kWh)	-	-	-	0.6785

The simulations were conducted using the NSGA-II algorithm within Pyomo, a Python-based framework for multi-objective optimisation [36]. The LL problem, formulated as a MILP problem, was implemented using Pyomo and solved with the Gurobi solver [52–54]. The NSGA-II algorithm was configured with a population size of 100, and 10,000 function evaluations were performed to obtain the Pareto-optimal solutions.

5.1. Numerical Results

In this subsection, the simulation results of the proposed MG design framework are presented and discussed, focusing on two key aspects: (1) the impact of frequency constraints on the design process,

and (2) the role of BESS on frequency control. The results provide insights into how frequency stability requirements influence the design and operation of the MG, as well as how integration of BESS affects the ability of the MG to meet demand while adhering to frequency requirements.

5.1.1. Impacts of frequency constraints

We considered the following two MG design methods for comparison to verify the need to include frequency constraints. Note that for a fair comparison, the proposed UL problem is the same for both methods.

- **Conventional**: The conventional MG design approach neglects the frequency constraints provided in Section 3.3.2 in the LL problem. For a fair comparison, a minimum of 15% spinning reserves was considered for the conventional design methodology [27].
- **Proposed**: The proposed frequency-constrained MG design framework is one with the LL problem described in Section 3.3, that is, (68)-(69).

The Pareto front shown in Figure 3 illustrates the trade-offs between the NPC and EM for both proposed design approaches. As expected, reducing EM leads to higher costs, highlighting the financial implications of integrating more BESS with RES. However, the proposed approach with PFR (represented by open circles) resulted in solutions with slightly higher NPC and EM than those of the conventional approach (filled circles). For example, the lowest NPC for the proposed and conventional approaches are 0.102 \$/kWh and 0.097 \$/kWh, respectively. Furthermore, at an NPC of \$0.105/kWh, the proposed approach achieves an EM of 0.18 kg CO_2-e/kWh, which is approximately a 12% increase compared to the conventional solution at the same cost level. The slightly higher NPC and EM were primarily due to the additional BESS and spinning reserves required to ensure PFR compliance.

The inclusion of RES curtailment as a performance metric, visualised by the colour gradient in Figure 3, provides further insight into the operation and performance of the MG. In both approaches, higher EM (on the left side of the Pareto front) are associated with minimal RES curtailment (around 60% or less) due to greater reliance on DGs. In contrast, as the EM decreases and the NPC increases, the penetration of RES increases, leading to a higher RES curtailment. This trend is particularly evident in the proposed approach, where the RES curtailment reaches 170% for the lowest EM solutions (below 0.145 kg CO_2-e/kWh). In the conventional approach, the RES curtailment remains below 140% due to the lower capacity of RES.

To perform a more detailed analysis, representative solutions are extracted from the Pareto fronts of both techniques by employing the fuzzy decision-making method [55, 56] in Table 4. In this method, an

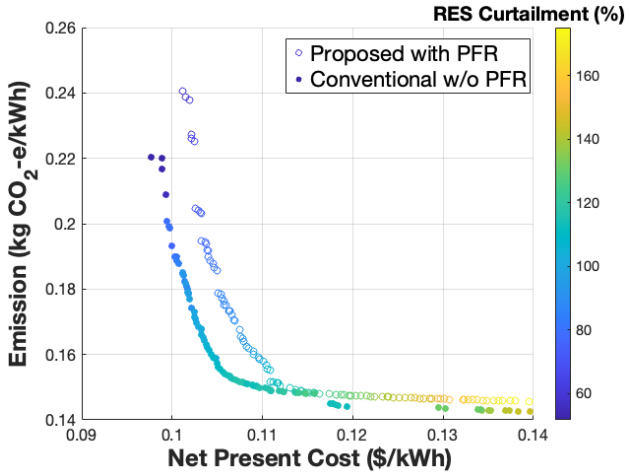

Figure 3: Pareto trade-offs between NPC and EM for the proposed and conventional approaches

equal weighting is considered for both NPC and EM, with the aim of achieving optimal compromises while adhering to frequency constraints. To offer a clearer benchmark for comparison, the results for DG-only cases are included for both the proposed and conventional approaches. This analysis underscores a critical observation: neglecting frequency stability requirements in MG design can lead to an undersized system that appears cheaper during planning but fails in real-world operation, causing operational challenges and inaccurate assessments of the project's economic viability. By incorporating renewable energy and frequency stability requirements, the proposed framework ensures a more realistic and robust MG design.

Table 4: Results of the selected MG design plans showing capacities, NPC, EM, and renewable energy curtailment (REC)

	Proposed with PFR		Conventional w/o PFR	
	DG-only	Hybrid	DG-only	Hybrid
P_{WT} (MW)	0	32	0	35
P_{PV} (MW)	0	14	0	14
P_{BT} (MW)	0	4.5	0	0
E_{BT} (MWh)	0	2.25	0	0
P_{DG} (MW)	22	13.8	12	12
NPC ($/kWh)	0.165	0.109	0.121	0.106
EM (kg CO_2-e/kWh)	0.881	0.161	0.685	0.154
REC (GWh/yr)	0	86	0	99

For the proposed design approach, the DG-only case is based entirely on DGs with a total capacity of 22 MW, almost twice the peak load. This results in an NPC of 0.165 $/kWh and EM of 0.881 kg CO_2-e/kWh with no renewable energy contribution. In contrast, the hybrid MG solution includes 32 MW of wind turbines, 14 MW of PV systems, and 4.5 MW/2.25 MWh of BESS, along with 13.8 MW of DGs. This combination reduces NPC and EM to 0.109 $/kWh and 0.161 kg CO_2-e/kWh, respectively, while curtailing

a significant amount of RES by up to 86 GWh/year (98% of annual energy demand).

For the conventional design approach, the DG-only case operated with a smaller 12 MW DG capacity, resulting in a lower NPC and EM, that is, 0.121 \$/kWh and 0.685 kg CO_2-e/kWh, respectively. In the hybrid MG solution, the system includes almost the same capacity of RES and DG as in the proposed model, i.e., 35 MW of wind turbines, 14 MW of PV systems, and 12 MW of DG, but without BESS. This resulted in a lower NPC (0.106 \$/kWh) and EM (0.154 kg CO_2-e/kWh), along with the highest RES curtailment of 99 GWh/year (113% of annual energy demand).

In general, DG-only cases demonstrate higher NPC and EM than hybrid MG solutions. Although the conventional approach yields lower NPC and EM for both cases, this outcome arises from ignoring operational requirements such as PFR constraints. By neglecting these constraints, the conventional approach underestimates the true cost, leading to operational challenges that affect the economic return of the project. Additionally, renewable energy curtailment is higher in the conventional hybrid MG solution, reaching 113% compared to 98% of the total demand in the proposed approach.

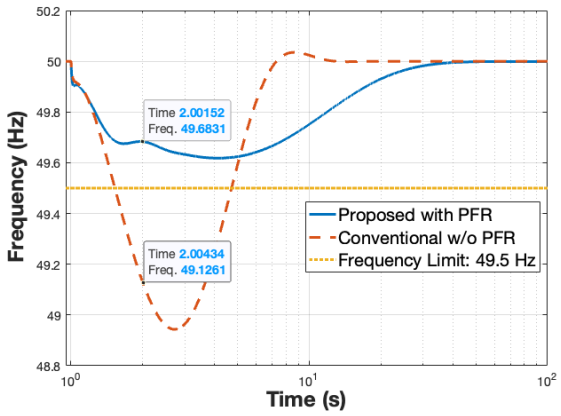

Figure 4: Frequency dynamics simulations at 10 PM on representative day 2 for the proposed and conventional hybrid design plans

The frequency responses of the selected MG designs with a mix of DERs, as described in Table 4, were further analysed using simulations in MATLAB/Simulink. Figure 4 illustrates the typical frequency response of the MG for the second representative day at 10 PM, following a sudden 15% increase in demand. The results reveal significant violations of the frequency stability metrics under conventional approach. In particular, the frequency nadir is 48.9 Hz, significantly lower than the typical threshold of 49.5 Hz. Moreover, within the initial second of the disturbance, the frequency decreased to 49.126 Hz, which corresponds to a RoCoF of 0.874 Hz/s. This value exceeded the predefined threshold.

To further analyse the frequency stability metrics, Figures 5 and 6 present the variations in the RoCoF and frequency nadir for all time intervals of representative days under both the proposed and conventional schemes. As demonstrated, the proposed methodology effectively maintains both the frequency nadir and RoCoF within allowable thresholds throughout the sample day, specifically $RoCoF_{\max} = 0.5\,\text{Hz/s}$ and $f_{\min} = 49.5\,\text{Hz}$.

In contrast, the conventional approach shows significant violations of the maximum RoCoF threshold in all time intervals of representative days 1, 2, and 5, as highlighted in the red boundary regions in Figure 5. Furthermore, Figure 6 indicates that the conventional approach frequently breaches the minimum frequency threshold, with violations occurring more than 60% of the time. These results highlight the essential role of integrating frequency stability constraints within the MG design framework to ensure secure and reliable system operation during unexpected disturbances.

Although the proposed design approach incurs slightly higher NPC due to the enforcement of higher inertia levels and PFR capabilities, these additional NPC can be justified by the secure and reliable operation in real time. Improvements in frequency stability are critical to mitigate power disturbances and ensure system reliability, particularly in the case of off-grid MGs for critical industries. Therefore, despite the marginal increase in NPC and EM, the proposed approach delivers superior frequency security, highlighting its value in robust MG operations.

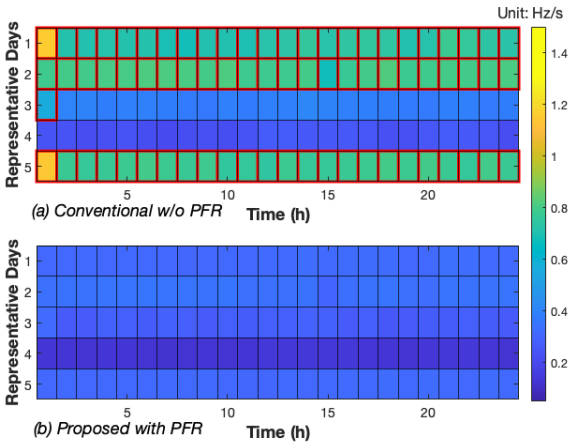

Figure 5: Post-disturbance RoCoF in all time intervals in each representative day for the proposed and conventional hybrid design plans, unacceptable values shown with red boundaries

5.1.2. Role of BESS on frequency control

For further analysis, we compare the proposed MG design model with a case in which only the synchronous generators are responsible for providing the PFR (that is, DG-based PFR) [57]. This study aims

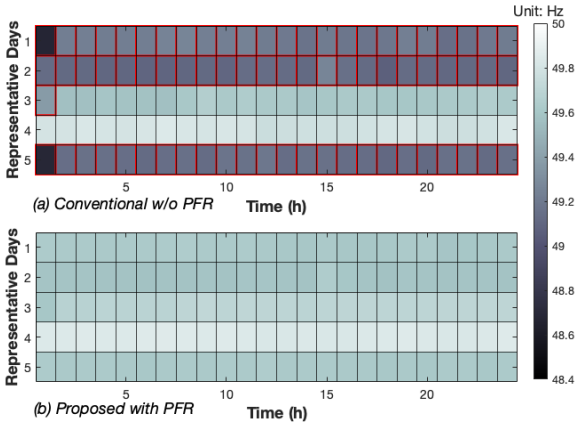

Figure 6: Post-disturbance frequency nadir in all time intervals in each representative day for the proposed and conventional hybrid design plans, unacceptable values shown with red boundaries

to evaluate the benefits of using BESS for PFR compared to employing BESS for energy arbitrage only and assigning PFR responsibilities to the fossil fuel generators.

Figure 7 illustrates the Pareto trade-offs between NPC and EM for the proposed system with PFR and DG-based PFR approaches. Relying exclusively on DGs for the PFR provision noticeably increases both NPC and EM. The primary reason is that the BESS is used solely for energy arbitrage and decreasing RES curtailment, which requires the installation of oversized DGs units to meet PFR needs. In addition, DGs must run under the no-load condition at all times to provide spinning reserves, resulting in higher EM.

In contrast, the proposed approach with PFR demonstrates a more favourable trade-off, achieving lower EM and NPC by using the BESS for both energy arbitrage and PFR provision. This highlights the dual benefit of incorporating BESS for grid support, as it reduces reliance on DGs and optimises the use of renewable energy, as evidenced by the lower percentages of RES curtailment shown in Figure 7.

5.2. Sensitivity Analysis

There are several parameters and assumptions that can influence planning results. This subsection provides a sensitivity analysis on two of the most important parameters, i.e., BESS cost and diesel fuel price.

5.2.1. Cost of BESS

As previously discussed, adding BESS can reduce emissions but increases the total NPC of the design. However, a recent analysis by NREL estimates that the future cost of BESS will decrease substantially [58]. The NREL report presents three BESS cost projection scenarios—low, mid, and high—indicating that the

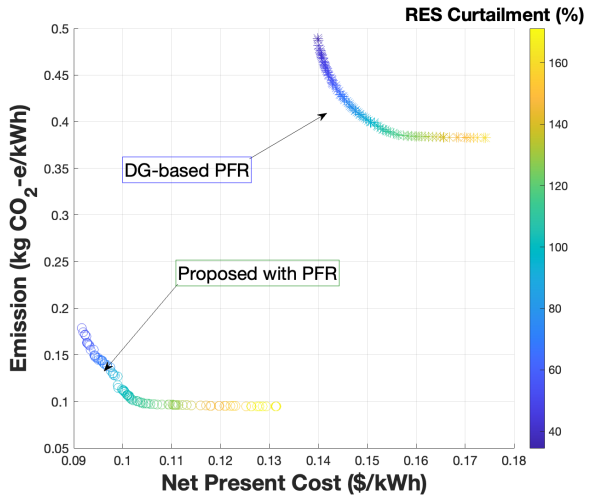

Figure 7: Pareto trade-offs between NPC and EM for the proposed design method with PFR and the DG-based PFR methodology

capital costs for energy and power components are expected to decline by 50%-47%, 38%-13%, and 20%-7%, respectively, by 2030 compared to 2022. Therefore, based on NREL projections for decreasing BESS capital costs, further simulations were conducted to quantify the impact of the proposed method.

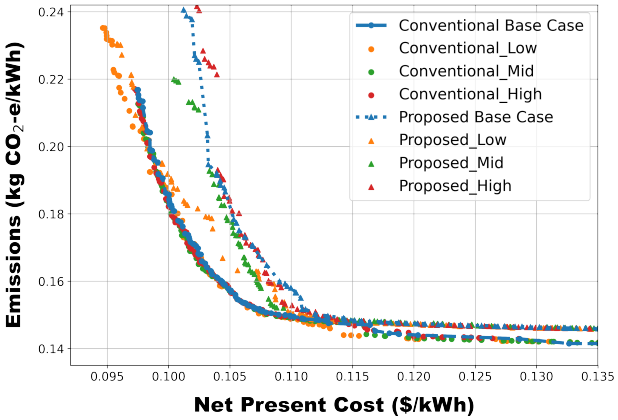

Figure 8: Pareto trade-offs between NPC and EM for the proposed and conventional approaches under low, mid, and high BESS cost projection scenarios

Figure 8 presents the Pareto fronts of NPC versus GHG emissions for the proposed and conventional approaches under three BESS cost projection scenarios: low, mid, and high. This comparison evaluates scenarios both with and without participation in PFR, highlighting the trade-offs between economic and environmental performance across different battery price assumptions. As shown, a decrease in BESS cost leads to a reduction in NPC for both approaches. However, the proposed method exhibits a more significant cost reduction due to greater BESS utilisation—particularly for PFR provision. In contrast, the conventional

approach rarely prefers BESS, even under low-cost scenarios, due to limited economic benefit without PFR participation. This results in closely clustered Pareto fronts across different cost cases for the conventional model.

These observations are further supported by the detailed results in Table 5, which summarises the selected optimal MG design obtained using the fuzzy decision-making method. In the conventional approach, no BESS is installed in the mid and high cost scenarios. Even in the low-cost scenario (50%-47% cost reduction in BESS), only a small BESS capacity (0.69 MW–0.88 MWh) found to be optimal. In contrast, the proposed approach shows significant BESS investment across all scenarios: 12.47 MW–6.91 MWh (low), 7.46 MW–5.93 MWh (mid), and 4.4 MW–3.12 MWh (high). This investment enables reduced reliance on diesel generators, with installed DG capacity dropping to 12 MW, 13.3 MW, and 13.5 MW, respectively.

Table 5: Results of the selected MG design for the proposed and conventional approaches under different BESS capital cost scenarios

	Proposed with PFR			Conventional w/o PFR		
	Low	Mid	High	Low	Mid	High
P_{WT} (MW)	34	36	36	33	36	36
P_{PV} (MW)	12	13	17	15	14	14
P_{BT} (MW)	12.47	7.46	4.4	0.69	0	0
E_{BT} (MWh)	6.91	5.93	3.12	0.88	0	0
P_{DG} (MW)	12.0	13.3	13.5	12.1	12.0	12.0
NPC ($/kWh)	0.106	0.112	0.115	0.104	0.106	0.106
EM (kg CO_2-e/kWh)	0.163	0.155	0.148	0.159	0.155	0.155
REC (GWh/yr)	84	95	105	90	98	98

5.2.2. Price of diesel fuel

Another important parameter in MG planning for mines is the diesel fuel price. Currently, the fuel cost for diesel generators is $0.17/kWh, which typically corresponds to a diesel price of $0.85 per litre [59]. This price includes a 50% rebate received by mining companies, which may be removed in the future. Additionally, diesel prices are highly volatile due to fluctuations in global oil markets and could increase or decrease significantly. For instance, in 2021, diesel prices were 40% higher, a trend that could re-occur in the future [60]. Therefore, a sensitivity analysis is conducted in this subsection considering two scenarios: (i) eliminating the 50% rebate ($1.7/litre), and (ii) a 40% increase in diesel price while maintaining the 50% rebate ($1.19/litre). We choose to analyse higher diesel prices because it is the more likely scenarios that is also motivating miners to force electrification and derive the original equipment manufacturer (OEM) industry to design new machinery and products.

Figure 9 illustrates the Pareto frontiers representing the trade-offs between NPC and GHG emissions

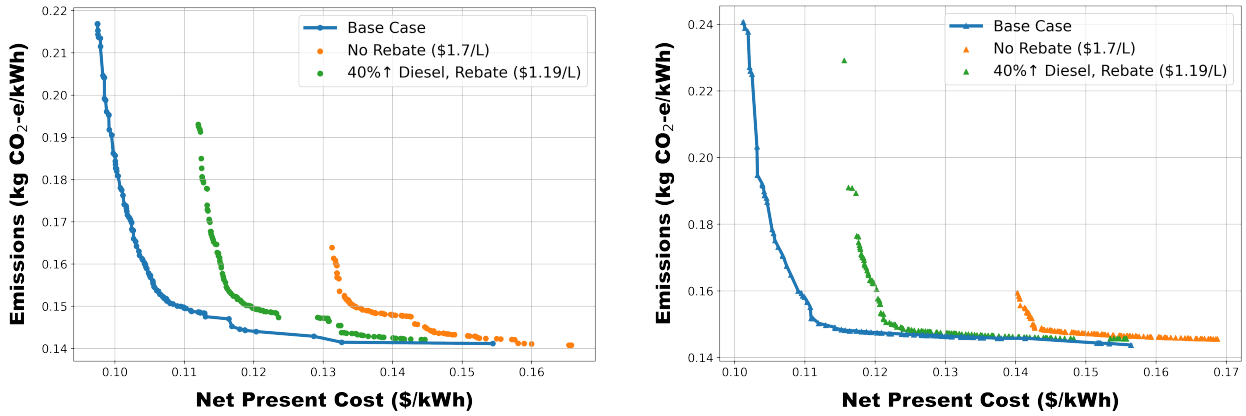

(a) Conventional w/o PFR

(b) Proposed with PFR

Figure 9: Pareto fronts of NPC versus EM under two diesel pricing scenarios for the conventional and proposed PFR-supported approaches.

for both the proposed and conventional approaches under two diesel pricing scenarios. The figure clearly highlights the influence of diesel pricing on MG design, comparing configurations with and without the provision of PFR. The Base Case—which assumes the current diesel price and rebate structure—unsurprisingly offers the lowest NPC (down to \$0.10/kWh) and the highest emissions (up to 0.24 kg CO_2-e/kWh) for both approaches. In the no-rebate scenario, where diesel is priced at \$1.70/L, the Pareto fronts shift downward and to the right, indicating increased costs and lower emissions compared to the Base Case and the other scenario due to lower utilisation and dependence on expensive diesel generation. Conversely, the scenario with a 40% increase in diesel price while retaining the rebate (\$1.19/L) yields intermediate outcomes, with slightly higher NPC and lower emissions compared to the base case, yet still more favourable than the no-rebate case.

Additionally, rising diesel prices enhance the economic viability of BESS. This trend is evident in the optimal MG configurations obtained via the fuzzy decision-making approach, as detailed in Table 6. For example, under the no-rebate scenario, even the conventional approach—which previously avoided BESS investment despite a 50% cost reduction—now incorporates 1.45 MW/3.13 MWh of BESS. Notably, the proposed method, when compared to the Base Case results in Table 4, triples its BESS capacity to further reduce DG sizing. This leads to lower DG utilisation and, consequently, reduced emissions. The outcome of the two sensitivity studies shows the importance of diesel prices in switching to BESS under both conventional and proposed methods, an impact that is more than the cost of BESS itself. These findings demonstrate the strong sensitivity of both techno-economic and environmental performance to diesel pricing policies, underscoring the critical role of supportive policy frameworks in enabling cost-effective, low-emission MG

solutions.

Table 6: Results of the selected MG design plans for the proposed and conventional approaches under diesel price scenarios

	Proposed with PFR		Conventional w/o PFR	
	No rebate	40% higher, rebate	No rebate	40% higher, rebate
P_{WT} (MW)	36	36	36	36
P_{PV} (MW)	17	17	17	15
P_{BT} (MW)	11.59	3.54	1.45	0
E_{BT} (MWh)	5.83	3.23	3.13	0
P_{DG} (MW)	13.1	13.4	12	12
NPC ($/kWh)	0.144	0.126	0.138	0.117
EM (kg CO_2-e/kWh)	0.148	0.148	0.148	0.152
REC (GWh/yr)	103	106	105	102

5.3. Computational Complexity and Convergence Analysis

The proposed framework utilises the NSGA-II algorithm to solve the multi-objective bi-level problem, where the UL problem determines the optimal planning decisions, and the LL problem deals with operational decisions, modelled as a MILP. This subsection evaluates the computational complexity and convergence characteristics of the approach. Moreover, we compare the performance and results obtained by executing four different evolutionary algorithms across three MG planning models: (i) Proposed with PFR, (ii) Conventional without PFR, and (iii) MG Planning DG-based PFR.

5.3.1. Computational complexity

As mentioned before, the main computational complexity of the proposed methodology arises from solving the LL problem multiple times within the UL problem. The complexity of the LL MILP problem is investigated in terms of the number of binary and continuous variables, constraints, and average solution time in Table 7. The values are reported for the proposed model with PFR, the conventional model without PFR, and the MG design model in which PFR is provided solely by the DGs.

The numbers in the table demonstrates that the proposed model incorporating PFR features the most number of variables and constraints, resulting in an average solution time of 28.86 seconds, which is considerably longer than the 11.12 seconds required by the conventional model. This increase is attributed to the additional requirements for PFR capabilities, which require more intricate constraints and variables. Despite the increased complexity, the proposed approach ensures compliance with the frequency stability requirements, which justifies the computational effort.

Table 7: Complexity metrics of the LL MILP problem

	Proposed with PFR	Conventional w/o PFR	MG planning DG-based PFR
# of continuous variables	66,251	24,481	37,451
# of binary variables	18,720	17,280	18,720
# of constraints	169,921	47,521	87,841
Average solution time (s)	28.86	11.12	20.30
MIP gap (%)	0.1	0.1	0.1
Time limit (s)	60	60	60

5.3.2. Convergence analysis

The convergence of NSGA-II was monitored using metrics such as hypervolume (HV), generational distance (GD), and inverted generational distance (IGD). These metrics assess the quality and diversity of the Pareto front over successive generations. In this regard, the above-mentioned MG design methodologies were run 10 times with different starting points using varying seed values.

Figure 10 illustrates the convergence trend of the HV, GD, and IGD metrics between generations, demonstrating a steady improvement in the quality of the Pareto front. Additionally, the computation time per generation stabilised after a few initial iterations, indicating the efficiency of the proposed enhancements.

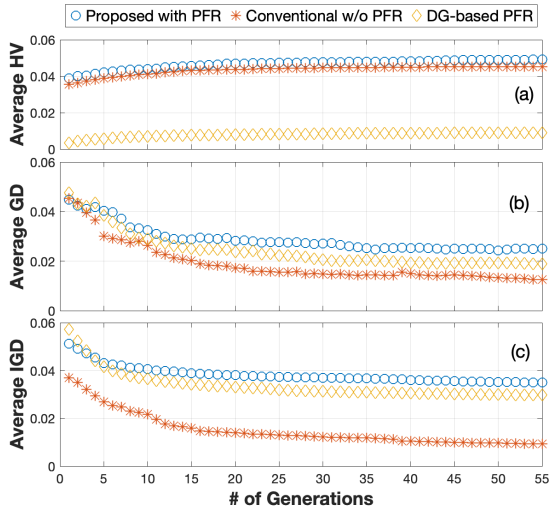

Figure 10: Average values of quality and diversity metrics over generations for MG design models, (a) Hyper volume, (b) Generational distance, and (c) Inverted generational distance

5.3.3. Evolutionary algorithm comparison

This subsection presents a comparison between the performance of NSGA-II and four other advanced evolutionary algorithms—NSGA-III, S-metric selection evolutionary algorithm (SMS-EMOA), adaptive geom-

etry estimation multi objective evolutionary algorithm (AGE-MOEA), and its newer version AGE-MOEA-II—to assess their performance in solving the bi-level MG planning problem. To ensure a fair comparison, all algorithms were executed on the same machine under identical settings, including a population size of 50 and 2500 function evaluations. Furthermore, each algorithm was executed 11 times using different random seed values to account for the stochastic nature of evolutionary algorithms' initiation.

Table 8: Comparison of evolutionary algorithms for different MG planning models

Model	Algorithm	HV	IGD	GD	RunTime (h)
Proposed with PFR	NSGA-II	**0.0453**	**0.0027**	0.0037	20.38
	NSGA-III	0.0439	0.0036	**0.0013**	**19.51**
	AGE-MOEA	0.0448	0.0030	0.0015	20.10
	AGE-MOEA-II	0.0445	0.0031	0.0020	20.44
	SMS-EMOA	0.0443	**0.0027**	**0.0013**	19.78
Conventional w/o PFR	NSGA-II	**0.0474**	0.0034	0.0027	8.42
	NSGA-III	0.0469	0.0033	0.0023	7.67
	AGE-MOEA	0.0468	**0.0033**	**0.0020**	**7.33**
	AGE-MOEA-II	0.0472	0.0034	0.0023	7.53
	SMS-EMOA	0.0469	0.0037	0.0025	7.67
MG planning DG-based PFR	NSGA-II	**0.0074**	**0.0031**	0.0031	14.65
	NSGA-III	0.0069	0.0047	0.0030	14.55
	AGE-MOEA	0.0072	0.0035	0.0032	13.86
	AGE-MOEA-II	**0.0074**	**0.0031**	0.0029	**13.45**
	SMS-EMOA	0.0071	0.0042	**0.0026**	13.98

Table 8 summarises the results across three MG planning models using average values of four key performance indicators: HV to measure convergence and diversity (higher value is preferred), IGD and GD to indicate closeness to the true Pareto front (lower value is better), and runtime in hours. For each model, the algorithm achieving the highest HV and the lowest IGD, GD, and runtime is highlighted in bold.

In the proposed with PFR model, NSGA-II achieves the best HV and IGD, while SMS-EMOA provides the lowest GD. NSGA-III exhibits the shortest runtime. For the conventional without PFR model, NSGA-II leads in HV, whereas AGE-MOEA shows superiority across IGD, GD, and runtime. In the DG-based PFR model, NSGA-II and AGE-MOEA-II share the highest HV, SMS-EMOA again achieves the lowest GD, and AGE-MOEA-II is the most computationally efficient.

These results highlight the trade-offs between solution quality and computational effort across different algorithmic strategies, offering valuable insights for selecting the most suitable optimisation technique based on specific planning objectives. However, the overall performance of these evolutionary algorithms is relatively close, suggesting that switching between them may not yield substantial improvements in the evaluated metrics.

6. Summary and Conclusions

This paper presents a frequency-constrained MG design framework tailored for heavy industries, such as mining, with a high penetration of renewable energy. The model, formulated as a multi-objective bi-level optimisation problem, determines the optimal sizing of solar, wind, BESS, and fossil fuel backup generators while ensuring frequency stability through metrics such as RoCoF, minimum/maximum frequency, and steady-state frequency. By addressing economic and operational objectives, including minimising NPC, reducing GHG emissions, improving the reliability of the system, and accounting for the degradation of the BESS, the model ensures reliable and cost-effective MG operation.

A case study of an off-grid underground mine in Australia is conducted to evaluate the proposed framework against two conventional approaches: MG design without PFR constraints and MG design with PFR provided solely by fossil fuel generators. The findings underscored the importance of integrating frequency constraints, as omitting them in conventional methods resulted in frequency deviations in more than 60% of the time, with nadirs reaching as low as 48.9 Hz and RoCoF peaking at 0.875 Hz/s—both outside acceptable limits. In contrast, the proposed method maintained frequency within the prescribed limits ($\geq$49.5 Hz and $\leq$0.5 Hz/s) at all times. While the proposed model led to a slightly higher NPC of 0.109 \$/kWh and GHG emissions of 0.161 kg CO_2-e/kWh, compared to 0.106 \$/kWh and 0.154 kg CO_2-e/kWh in the conventional method, it significantly improved operational reliability and reduced RES curtailment by 13% due to the utilisation of BESS for both PFR and energy arbitrage. Furthermore, excluding BESS from the PFR provision resulted in oversized fossil fuel generators, increased NPC, and higher GHG emissions. These findings underscore the critical role of BESS in improving frequency stability and achieving superior economic and environmental outcomes.

Future work will focus on linearising the BESS degradation model to enable single-level optimisation, incorporating voltage and network constraints for improved design accuracy, and integrating different types of BESS for specialised roles, such as long-term energy arbitrage and short-term frequency support. Additionally, modelling RES uncertainties and fluctuations in the mining MG design in a computationally tractable manner is another necessary direction for future studies. Doing so can improve the feasibility and robustness of the proposed solutions under real-world operational variability. These advances aim to further optimise the MG planning process, ensuring greater efficiency, reliability, and sustainability in industrial applications.

Acknowledgment

This work was supported by the University of Adelaide through the Mine Operational Vehicle Electrification (MOVE) project, funded by the Future Battery Industries Cooperative Research Centre as part of the Commonwealth Cooperative Research Centre Program. During the preparation of this work, the authors used ChatGPT in order to improve readability and language. After using this tool, the authors reviewed and edited the content as needed and take full responsibility for the content of the publication.

References

[1] H. Assimi, S. N. H. Ataabadi, S. M. M. Islam, W. L. Soong, S. A. Pourmousavi, Toward underground mobile fleet electrification: Three essential steps to make a real change, IEEE Electrification Magazine 12 (1) (2024) 16–26.

[2] J. J. Guilbaud, Hybrid renewable power systems for the mining industry: System costs, reliability costs, and portfolio cost risks, Ph.D. thesis, UCL (University College London) (2016).

[3] A. Pourmousavi, H. Assimi, W. Soong, B. Foley, S. N. Hashemian, S. M. M. Islam, An overview of Australia's mining vehicle and mining equipment electrification, Tech. rep., Future Battery Industries Cooperative Research Centre (2023).
URL https://fbicrc.com.au/wp-content/uploads/2023/11/FBICRC_Mobile-Mine-Report-VFINAL.pdf

[4] L. Delevingne, W. Glazener, L. Grégoir, K. Henderson, Climate risk and decarbonization: What every mining CEO needs to know, Report McKinsey & Company.

[5] G. Alova, Integrating renewables in mining: Review of business models and policy implications.

[6] N. Ertugrul, A. P. Kani, M. Davies, D. Sbarbaro, L. Morán, Status of mine electrification and future potentials, in: 2020 International Conference on Smart Grids and Energy Systems (SGES), IEEE, 2020, pp. 151–156.

[7] J. Webb, H. N. de Silva, C. Wilson, The future of coal and renewable power generation in Australia: a review of market trends, Economic Analysis and Policy 68 (2020) 363–378.

[8] SunSHIFT Pty Ltd, Renewable energy in the Australian mining sector, Tech. rep., Australian Renewable Energy Agency (2017).
URL https://arena.gov.au/assets/2017/11/renewable-energy-in-the-australian-mining-sector.pdf

[9] Australian Renewable Energy Agency (ARENA), Hybrid power generation for Australian off-grid mines, Tech. rep., Australian Renewable Energy Agency (2018).
URL https://arena.gov.au/assets/2018/06/hybrid-power-generation-australian-off-grid-mines.pdf

[10] X. Zhu, B. Mather, P. Mishra, Grid impact analysis of heavy-duty electric vehicle charging stations, in: 2020 IEEE Power & Energy Society Innovative Smart Grid Technologies Conference (ISGT), IEEE, 2020, pp. 1–5.

[11] X. Zhu, R. Mahmud, B. Mather, P. Mishra, A. Meintz, Grid voltage control analysis for heavy-duty electric vehicle charging stations, in: 2021 IEEE Power & Energy Society Innovative Smart Grid Technologies Conference (ISGT), IEEE, 2021, pp. 1–5.

[12] Epiroc, Minetruck MT42 battery technical specification.

[13] G. B. Kumar, R. K. Sarojini, K. Palanisamy, S. Padmanaban, J. B. Holm-Nielsen, Large scale renewable energy integration: Issues and solutions, Energies 12 (10) (2019) 1996.

[14] B. Bacha, H. Ghodbane, H. Dahmani, A. Betka, A. Toumi, A. Chouder, Optimal sizing of a hybrid microgrid system using solar, wind, diesel, and battery energy storage to alleviate energy poverty in a rural area of Biskra, Algeria, Journal of Energy Storage 84 (2024) 110651.

[15] S. Forrousso, S. I. Kaitouni, A. Mana, M. Wakil, A. Jamil, J. Brigui, H. Azzouzi, Optimal sizing of off-grid microgrid building-integrated-photovoltaic system with battery for a net zero energy residential building in different climates of Morocco, Results in Engineering 22 (2024) 102288.

[16] F. A. Kassab, B. Celik, F. Locment, M. Sechilariu, S. Liaquat, T. M. Hansen, Optimal sizing and energy management of a microgrid: A joint MILP approach for minimization of energy cost and carbon emission, Renewable Energy 224 (2024) 120186.

[17] X. Zhu, G. Ruan, H. Geng, H. Liu, M. Bai, C. Peng, Multi-objective sizing optimization method of microgrid considering cost and carbon emissions, IEEE Transactions on Industry Applications 60 (4) (2024) 5565–5576.

[18] O. Ellabban, A. Alassi, Optimal hybrid microgrid sizing framework for the mining industry with three case studies from Australia, IET Renewable Power Generation 15 (2) (2021) 409–423.

[19] A. Maronga, K. J. Nyoni, P. G. Tuohy, A. Shane, Evaluation of PV and CSP systems to supply power in the Zimbabwe mining sector, Energies 14 (13) (2021) 3740.

[20] J. Vergara-Zambrano, W. Kracht, F. A. Díaz-Alvarado, Integration of renewable energy into the copper mining industry: A multi-objective approach, Journal of Cleaner Production 372 (2022) 133419.

[21] Y. Wen, W. Li, G. Huang, X. Liu, Frequency dynamics constrained unit commitment with battery energy storage, IEEE Transactions on Power Systems 31 (6) (2016) 5115–5125.

[22] S. Yan, Y. Zheng, D. J. Hill, Frequency constrained optimal siting and sizing of energy storage, IEEE Access 7 (2019) 91785–91798.

[23] S. Córdova, C. A. Cañizares, À. Lorca, D. E. Olivares, Frequency-constrained energy management system for isolated microgrids, IEEE Transactions on Smart Grid 13 (5) (2022) 3394–3407.

[24] B. Jiang, C. Guo, Z. Chen, Frequency constrained unit commitment considering reserve provision of wind power, Applied Energy 361 (2024) 122898.

[25] S. Cai, Y. Xie, Y. Zhang, W. Bao, Q. Wu, C. Chen, J. Guo, Frequency constrained proactive scheduling for secure microgrid formation in wind power penetrated distribution systems, IEEE Transactions on Smart Grid 16 (2) (2025) 989–1002.

[26] H. Li, H. Zhang, D. Liu, J. Zhang, C.-K. Wong, Frequency-constrained dispatching for an integrated electricity-heat microgrid with synergic regulation resources, IEEE Transactions on Industry Applications 61 (2) (2025) 2203–2215.

[27] M. Javadi, Y. Gong, C. Chung, Frequency stability constrained BESS sizing model for microgrids, IEEE Transactions on Power Systems 39 (2) (2023) 2866–2878.

[28] M. Bayat, M. G. Farahani, A. A. Ghadimi, M. Tostado-Veliz, M. R. Miveh, F. Jurado, Optimal siting, sizing and setting of droop-controlled DERs in autonomous microgrids: A new paradigm in microgrid planning, Electric Power Systems Research 225 (2023) 109850.

[29] J. M. Rey, I. Jiménez-Vargas, P. P. Vergara, G. Osma-Pinto, J. Solano, Sizing of an autonomous microgrid considering droop control, International Journal of Electrical Power & Energy Systems 136 (2022) 107634.

[30] L. Yang, H. Li, H. Zhang, Q. Wu, X. Cao, Stochastic-distributionally robust frequency-constrained optimal planning for an isolated microgrid, IEEE Transactions on Sustainable Energy.

[31] H. Li, H. Zhang, J. Zhang, Q. Wu, C.-K. Wong, A frequency-secured planning method for integrated electricity-heat microgrids with virtual inertia suppliers, Applied Energy 377 (2025) 124540.

[32] Y. Wang, G. Strbac, A planning model for the optimal sizing of integrated power and gas systems capturing frequency security, CSEE Journal of Power and Energy Systems.

[33] S. Sitompul, G. Fujita, Impact of advanced load-frequency control on optimal size of battery energy storage in islanded microgrid system, Energies 14 (8) (2021) 2213.

[34] K. S. El-Bidairi, H. D. Nguyen, T. S. Mahmoud, S. Jayasinghe, J. M. Guerrero, Optimal sizing of battery energy storage systems for dynamic frequency control in an islanded microgrid: A case study of Flinders Island, Australia, Energy 195 (2020) 117059.

[35] T. Igogo, K. Awuah-Offei, A. Newman, T. Lowder, J. Engel-Cox, Integrating renewable energy into mining operations: Opportunities, challenges, and enabling approaches, Applied Energy 300 (2021) 117375.

[36] J. Blank, K. Deb, Pymoo: Multi-objective optimization in python, IEEE Access 8 (2020) 89497–89509. doi:10.1109/ACCESS.2020.2990567.

[37] M. A. Abdoulaye, S. Waita, C. W. Wekesa, J. M. Mwabora, Optimal sizing of an off-grid and grid-connected hybrid photovoltaic-wind system with battery and fuel cell storage system: A techno-economic, environmental, and social assessment, Applied Energy 365 (2024) 123201.

[38] K. Smith, P. Gasper, Battery lifetime analysis and simulation tool - lite (BLAST-Lite) (2023).
URL https://www.osti.gov//servlets/purl/1992056

[39] P. Kundur, Power system stability, Power system stability and control 10 (2007) 7–1.

[40] Y. Wen, C. Guo, D. S. Kirschen, S. Dong, Enhanced security-constrained OPF with distributed battery energy storage, IEEE Transactions on Power Systems 30 (1) (2014) 98–108.

[41] A. Heydari, A. Askarzadeh, Techno-economic analysis of a PV/biomass/fuel cell energy system considering different fuel cell system initial capital costs, Solar energy 133 (2016) 409–420.

[42] B. Ahmadi, O. Ceylan, A. Ozdemir, M. Fotuhi-Firuzabad, A multi-objective framework for distributed energy resources planning and storage management, Applied Energy 314 (2022) 118887.

[43] M. Lambert, R. Hassani, Diesel genset optimization in remote microgrids, Applied Energy 340 (2023) 121036.

[44] F. Teng, V. Trovato, G. Strbac, Stochastic scheduling with inertia-dependent fast frequency response requirements, IEEE Transactions on Power Systems 31 (2) (2015) 1557–1566.

[45] H. Chávez, R. Baldick, S. Sharma, Governor rate-constrained OPF for primary frequency control adequacy, IEEE Transactions on Power Systems 29 (3) (2014) 1473–1480.

[46] H. D. Sherali, W. P. Adams, A reformulation-linearization technique for solving discrete and continuous nonconvex problems, Vol. 31, Springer Science & Business Media, 2013.

[47] Supplementary document, accessed: 2024-09-18.
URL http://dx.doi.org/10.13140/RG.2.2.11454.50240

[48] IEEE PES Industry Technical Support Leadership Committee, Impact of IEEE 1547 standard on smart inverters and the applications in power systems, Tech. rep., National Renewable Energy Laboratory (NREL) (2020).
URL https://www.nrel.gov/media/docs/libraries/grid/smart-inverters-applications-in-power-systems.pdf

[49] Energy Transformation Taskforce, Western Australia, Revising frequency operating standards in the SWIS, Tech. rep., Energy Transformation Taskforce, Western Australia (2019).

[50] GHD Advisory, System rate of change of frequency, a GHD survey of international views, Tech. rep., Australian Energy Market Commission (AEMC) (2023).

[51] Australian Energy Market Commission (AEMC), The frequency operating standard for the NEM – stage one (final), Tech. rep., Australian Energy Market Commission (AEMC) (2017).

[52] M. L. Bynum, G. A. Hackebeil, W. E. Hart, C. D. Laird, B. L. Nicholson, J. D. Siirola, J.-P. Watson, D. L. Woodruff, et al., Pyomo-optimization modeling in Python, Vol. 67, Springer, 2021.

[53] W. E. Hart, J.-P. Watson, D. L. Woodruff, Pyomo: modeling and solving mathematical programs in python, Mathematical Programming Computation 3 (2011) 219–260.

[54] Gurobi Optimization, LLC, Gurobi Optimizer Reference Manual (2024).
URL https://www.gurobi.com

[55] H. Saber, M. Moeini-Aghtaie, M. Ehsan, Developing a multi-objective framework for expansion planning studies of distributed energy storage systems (DESSs), Energy 157 (2018) 1079–1089.

[56] H. Saber, H. Ranjbar, H. Mazaheri, A stochastic multi-objective planning framework for distributed energy resources as an alternative to transmission expansion, in: 2024 IEEE Texas Power and Energy Conference (TPEC), IEEE, 2024, pp. 1–6.

[57] A. M. Nakiganda, S. Dehghan, U. Markovic, G. Hug, P. Aristidou, A stochastic-robust approach for resilient microgrid investment planning under static and transient islanding security constraints, IEEE Transactions on Smart Grid 13 (3) (2022) 1774–1788.

[58] C. Murray, Li-ion bess costs could fall 47% by 2030, NREL says in long-term forecast update (2023).
URL https://www.energy-storage.news/li-ion-bess-costs-could-fall-47-by-2030-nrel-says-in-long-term-forecast-update/

[59] Generator Source, Fuel consumption charts, accessed: 2025-05-07.
URL https://generatorsource.com/tools-info/fuel-consumption-charts/

[60] GlobalPetrolPrices.com, Australia diesel prices, accessed: 2025-04-24 (2025).
URL https://www.globalpetrolprices.com/Australia/diesel_prices/